Final Technical Report Title:	Cooling Strategies for Vane Leading Edges in a Syngas Environment Including Effects of Deposition and Turbulence
Reporting Period Start/End Date:	1 October 2010 – 30 September 2014
UND Principal Investigator:	Forrest E. Ames, PhD, Professor Department of Mechanical Engineering University of North Dakota 243 Centennial Drive Grand Forks, ND 58202 (701) 777-2095, forrest.ames@engr.und.edu
Other UND Team Members:	Preethi Gandavarapu, Nafiz Chowhury, Juli Pearson, Mitch Busche, Joseph Kingery
OSU Principal Investigator:	Dr. Jeffrey Bons, Ohio State University Department of Aerospace Engineering The Ohio State University 2300 West Case Rd. Columbus, OH
Other OSU Team Members:	Carlos Bonilla and Carey Clum
Sponsor:	Department of Energy/National Energy Technology Laboratory
Project:	Award Number: DE-FE0004588
UND DUNS Number:	DUNS Number: 10-228-0781
Submitted by:	Forrest E. Ames 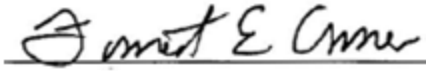
Submission Date:	9 February 2015
Distribution Notice:	Unlimited—No Restrictions

Disclaimer:

TABLE OF CONTENTS

3. ABSTRACT

The Department of Energy has goals to move land based gas turbine systems to alternate fuels including coal derived synthetic gas and hydrogen. Coal is the most abundant energy resource in the US and in the world and it is economically advantageous to develop power systems which can use coal. Integrated gasification combined cycles are (IGCC) expected to allow the clean use of coal derived fuels while improving the ability to capture and sequester carbon dioxide. These cycles will need to maintain or increase turbine entry temperatures to develop competitive efficiencies. The use of coal derived syngas introduces a range of potential contaminants into the hot section of the gas turbine including sulfur, iron, calcium, and various alkali metals. Depending on the effectiveness of the gas clean up processes, there exists significant likelihood that the remaining materials will become molten in the combustion process and potentially deposit on downstream turbine surfaces. Past evidence suggests that deposition will be a strong function of increasing temperature. Currently, even with the best gas cleanup processes a small level of particulate matter in the syngas is expected. Consequently, particulate deposition is expected to be an important consideration in the design of turbine components.

The leading edge region of first stage vanes most often have higher deposition rates than other areas due to strong fluid acceleration and streamline curvature in the vicinity of the surface. This region remains one of the most difficult areas in a turbine nozzle to cool due to high inlet temperatures and only a small pressure ratio for cooling. The leading edge of a vane often has relatively high heat transfer coefficients and is often cooled using showerhead film cooling arrays. The throat of the first stage nozzle is another area where deposition potentially has a strongly adverse effect on turbine performance as this region meters the turbine inlet flow. Based on roughness levels found on in service vanes (Bons, et al., 2001, up to 300 microns) flow blockage in first stage turbine nozzles can easily reach 1 to 2 percent in conventional turbines. Deposition levels in syngas fueled gas turbines are expected to be even more problematic.

The likelihood of significant deposition to the leading edge of vanes in a syngas environment indicates the need to examine this effect on the leading edge cooling problem. It is critical to understand the influence of leading edge geometry and turbulence on deposition rates for both internally and showerhead cooled leading edge regions. The expected level of deposition in a vane stagnation region not only significantly changes the heat transfer problem but also suggests that cooling arrays may clog. Addressing the cooling issue suggests a need to better understand stagnation region heat transfer with realistic roughness as well as the other variables affecting transport near the leading edge. Also, the question of whether leading edge regions can be cooled internally with modern cooling approaches should also be raised, thus avoiding the clogging issue. Addressing deposition in the pressure side throat region of the nozzle is another critical issue for this environment. Issues such as examining the protective effect of slot and full coverage discrete-hole film cooling on limiting deposition as well as the influence of roughness and turbulence on effectiveness should be raised. The objective of this present study is to address these technical challenges to help enable the development of high efficiency syngas tolerant gas turbine engines.

4. EXECUTIVE SUMMARY

The leading edge regions of airfoils in gas turbine engines are difficult to cool due to relatively high heat transfer rates combined with low local pressure ratios which drive the coolant flow. Normally, these regions are cooled using an array of slanted cooling holes called showerhead cooling. However, in environments where contaminants exist in the fuel (such as syn-gas) or air, these holes are susceptible for clogging which could potentially cause failure or reduced component life. This potential of showerhead and pressure surface holes to clog and the development of means to cool and protect the stagnation region and pressure surface has warranted the current investigation.

The development of methods to cool leading edge regions requires improved knowledge of heat transfer rates in the leading edge regions of land based gas turbines. Land based gas turbines have grown substantially with time while the relative diameter of leading edge regions has become larger. This growth has led to much higher Reynolds numbers. At the same time the development of dry low NOx combustion systems has often produced very high approach flow turbulence levels. The combination of high Reynolds numbers with high turbulence levels has produced stagnation region heat transfer conditions which were previously beyond the parameter range documented in the open literature. The current project has addressed this concern by substantially expanding the combined Reynolds number, turbulence level parameter range for leading edge region heat transfer. These new data will allow better heat transfer predictions for stagnation regions for large land based gas turbines.

This expanded parameter range has also produced questions regarding the influence of larger leading edge regions and higher turbulence levels on deposition rates in gas turbine. The present project has also addressed these two concerns using the turbine reacting flow rig (TuRFR) at the Ohio State University. In addition, the influence of full coverage slot film cooling has also been investigated at the Ohio State University to determine how well the pressure surface can be protected from deposition using film cooling. The work accomplished at OSU furthered the understanding of deposition effects on power turbines with the following significant contributions:

- Conclusive evidence was obtained experimentally that underscores the dominant role of particle Stokes number in determining particle-to-surface delivery and subsequent deposition. Thus, cylindrical objects with a diameter equivalent to a turbine vane leading edge will experience comparable deposition, all other conditions being the same.
- Since larger leading edge radius vanes decrease the effective Stokes number of airborne particles, they experience a lower deposition rate per unit area than smaller radius vanes.
- Freestream turbulence increases the delivery of particles to the surface and thus the particle deposition rate. Unexpectedly, smaller particles are less (not more, as anticipated) influenced by turbulence levels.
- Slot cooling is an effective means of mitigating deposition on a turbine nozzle guide vane. With slot cooling, deposition is reduced both upstream and downstream of the coolant slot. This is due to the substantial conduction cooling that takes place upstream of the coolant slot.

These conclusions and observations are of benefit to turbine designers as they consider the environmental impact of airborne impurities on turbine operation. Slot cooling could be implemented in a turbine design and substantial reductions in deposition will result. Also, the ability to anticipate deposition rates in regions of higher freestream turbulence could aid in repair and refurbishment of fowled turbine surfaces.

This project has also developed a new internal cooling method which can be used to cool leading edge regions of vanes without the use of showerhead cooling. This method is called incremental impingement and has been shown to be able to sustain relatively high internal cooling levels over a reasonably broad region on a surface. This development is noteworthy as elimination of showerhead cooling in the leading edge and discrete hole film cooling downstream substantially reduces the potential of these surfaces to clog which can lead to cooling system failure.

Additionally, during this project a well resolved database has been developed to document the influence of acceleration and turbulence on slot film cooling. This work conclusively demonstrates the dependency of downstream film cooling protection on local turbulence levels. This work is critical to the reliable application of slot film cooling for thermal and potentially deposition protection. A similarly comprehensive film cooling investigation was conducted for a double row full coverage array of shaped-holes.

This research is believed to offer the gas turbine community the combination of heat transfer and deposition predictive capabilities needed to address the use of large leading edge regions for new land based gas turbines. Additionally, this research is also believed to offer the gas turbine community a practical means to protect leading edge and pressure surface regions both thermally and from the unwanted buildup of deposition from contaminants in the fuel and air.

5. COMPARISON OF ACTUAL ACCOMPLISHMENTS WITH THE GOALS AND OBJECTIVES OF THE PROJECT.

The overall objective of this research project has been to develop the heat transfer and deposition predictive tools and surface protective cooling technologies which allow for the reliable design of leading edge cooling schemes in a syngas environment. This research also investigated the potential of full coverage film cooling to protect throat areas from build-up of significant blockage. The project goals include coupling deposition studies at OSU with external heat transfer, internal cooling, and film cooling studies at UND.

RESEARCH OBJECTIVES UND: The tasks to be accomplished by UND include; experimental stagnation region heat transfer studies over a range of turbulence and Reynolds number conditions, internal heat transfer studies, and external film cooling and heat transfer studies over a range of turbulence conditions at two Reynolds numbers.

Goal 1. UND will document the influence of leading edge diameter, Reynolds number and turbulence condition on stagnation region heat transfer.

Status: (Completed)

Discussion: This goal involved testing two large cylindrical leading edge test surfaces over an eight to one range in Reynolds numbers over a total of seven distinct turbulence conditions. The leading edge diameter approach flow Reynolds number was tested over Reynolds numbers ranging from 15,625 to 125,000 for the smaller leading edge surface and from 62,500 to 500,000 for the larger of the two leading edge surfaces. Turbulence levels ranging from 0.7% to 17.4% were developed for these tests with turbulent energy scales ranging from 1.8 cm to 9.5 cm. Turbulent augmentation levels of up to 136% were found. Originally, the two test surfaces were tested at 6 turbulence conditions. Later, after two attempts, a very high turbulence generator was developed and characterized and tested with the two leading edge test surfaces. This work resulted in two ASME IGTI papers which have been published or recommended for publication in the Journal of Turbomachinery.

Goal 2. UND will also study the stagnation region flow field including boundary layer development.

Status: (Completed)

Discussion: This goal involved documenting the response of turbulence approaching the two cylindrical leading edge test surfaces and acquiring boundary layer profiles off the surface downstream surface of the larger cylinder. Initially, a traversing system was set up on a thin low blockage plate that split the flow in the test section. The traversing system positioned a single element hot wire from a location consistent with the leading edge stagnation line to positions well upstream from the leading edge. These measurements were initially acquired for the test surface without the leading edge test surfaces in place and later the traversing mechanism was integrated into both the smaller and larger leading edge test surface to document the response of the different turbulence conditions to the presence of the cylinders. These measurements were documented in an ASME IGTI paper. The paper showed that the response of

the turbulence was affected by the blocking effect of the surface, the turbulence scale to diameter ratio, the effect of the cylinder on the convection time, and the turbulent time scale Lu/u'. Measurements of the boundary layers growing on the large cylindrical leading edge were acquired at about 30° from the stagnation line over a four to one range in Reynolds numbers. One student is currently working to document this work in her thesis.

Goal 3. UND will investigate the combined impact of turbulence and roughness due to deposition (OSU) on stagnation region heat transfer.
Status: (Not completed)
Discussion: This goal was not completed. We delayed this goal till the end of the project to enable heat transfer measurements on the larger and smaller leading edge test surfaces with the new very high turbulence generator. Subsequently, when we attempted to model the rough surface we ran into difficulties developing a solid model of the surface based on the previous modeling approach we had used. We ran out of time and were not able to overcome the issues involved in developing the solid model.

Goal 4. UND will conduct internal heat transfer studies for stagnation region cooling. (Done)
Status: (Completed)
Discussion: This goal involved developing a cooling concept which could cool a high heat load over an extended surface. Noting that cooling levels of typical internal cooling methods significantly decay as cooling air heats up, we developed a method the incrementally replenished the cooling air in a channel. We call this method incremental replenishment or incremental impingement. We designed, fabricated and tested two versions of this concept. This work was documented in an ASME IGTI paper which has been published in the Journal of Turbomachinery.

Goal 5. UND will investigate the influence of turbulence on downstream full coverage discrete hole and slot film cooling over smooth surfaces. (Smooth surface slot and shaped-hole film cooling completed)
Status: (Completed)
Discussion: Larger and smaller cylindrical leading edge test surfaces were fabricated to investigate the influence of turbulence, acceleration, and Reynolds number on slot film cooling. Adiabatic effectiveness and heat transfer data were acquired at six turbulence conditions, four blowing ratios and two Reynolds numbers for both test surfaces. This work showed the strong influence of turbulence condition, acceleration and Reynolds number on adiabatic effectiveness distributions. Heat transfer distributions were also affected by these variables but to a lesser extent. This research was documented in an ASME IGTI paper which was published last year. A double-row array of shaped holes was also tested on the larger cylindrical leading edge test surface. This array was tested over the same turbulence conditions, Reynolds numbers and flow rates as the 2D slot geometry. This research has also been documented in an ASME IGTI paper which has been accepted for publication and presentation at Turbo Expo 2015.

Goal 6. UND will investigate the influence of turbulence and the combined influence of roughness (from OSU deposition studies) and turbulence on downstream full coverage shaped hole and slot film cooling. (Rough surface slot and shaped-hole film cooling not completed)
Status: (Not completed)
Discussion: This goal was not completed. Similar to the rough surface stagnation heat transfer measurements, we delayed this goal until the end of the project to first allow heat transfer measurements on the larger and smaller leading edge test surfaces with the new very high turbulence generator. We ran out of time and were not able to complete this goal.
RESEARCH OBJECTIVES OSU: The tasks to be accomplished at OSU include; experimental deposition studies for various combinations of free-stream turbulence level, leading edge diameter, and coolant design. The work was divided into three specific phases. The specific objectives for each phase are listed below:

<u>Phase 1</u>. Develop a suitable test bed for deposition studies with different leading edge diameter.

1) Generate deposits on a turbine vane and on a faired cylinder stand-in. Determine if deposition mechanism is similar in LE region. Determine the conditions under which a faired cylinder is a good model for LE deposition on turbine vane. ACCOMPLISHED
2) Decision point:
    a. If a faired cylinder is NOT a good model – use vanes for study and seek other partners/hardware for larger LE radius vanes
    b. If a faired cylinder IS a good model – compare deposition on various LE radii cylinders at constant gas temp, inlet Mach, particulate type and loading. ACCOMPLISHED
3) Measure deposition rate, surface roughness, deposit thickness, and composition ACCOMPLISHED
4) Send deposit surfaces to UND for modeling ACCOMPLISHED

<u>Phase 2</u>. Explore influence of free-stream turbulence level on deposition

a. Since turbulent diffusion is known to be a significant mechanism for deposition in turbines, different freestream turbulence levels will be generated in the OSU TuRFR. ACCOMPLISHED
b. Study deposition rate for various turbulence level and leading edge diameter combinations ACCOMPLISHED
c. Measure deposition rate, surface roughness, deposit thickness, and composition ACCOMPLISHED
d. Send deposit surfaces to UND for modeling NOT ACCOMPLISHED
e. Explore use of infrared camera and cylinder-integrated thermocouples to determine the heat load during deposition as well as evolution of deposition under different flow conditions. ATTEMPTED BUT NOT SUCCESSFULLY ACCOMPLISHED

<u>Phase 3</u>. Explore use of film cooling to mitigate deposition in the leading edge region AND on pressure surface near passage throat.

a. Various cooling patterns will be explored on faired cylinders in the TuRFR to determine their effectiveness at mitigating deposition. STARTED BUT THEN DISCONTINUED IN FAVOR OF INVESTIGATING COOLING ON AN ACTUAL VANE (b).
b. An actual turbine vane will also be installed in the TuRFR to explore the effect of cooling on deposition in the leading edge and pressure surface region. ACCOMPLISHED
c. Send deposit surfaces to UND. NOT ACCOMPLISHED

6. SUMMARY OF PROJECT ACTIVITIES: ORIGINAL HYPOTHESIS THROUGH ASSESSMENT OF PROJECT IMPACT.

The overall focus of this project has been to develop and investigate technologies which have the potential to reliably cool and protect leading edge and pressure surfaces in a syngas environment. The original hypothesis suggested that even current and future technology syngas fired gas turbines will need to be tolerant of fuel and air-bound particulate deposition to allow reliable operation. Further, research at OSU has demonstrated that showerhead and pressure surface film cooling holes often provide sites where particulate deposition can gain a foothold. Subsequently, these holes have the potential to clog which can lead to cooling system failure. Consequently, cooling methods are needed, that can manage leading edge heat loads and protect pressure surfaces from deposition, which eliminate the use of showerhead cooling arrays and discrete-hole film cooling. The project activities were centered on supporting the performance of the key goals or tasks of the project developed to address this issue. The general approaches used by UND included heat transfer, film cooling and fluid dynamics testing in UND's large-scale low speed cascade facility and characterization of internal cooling methods in UND's internal heat transfer and flow

rig. The general approaches used by OSU included accelerated deposition testing, turbulence measurements, and film cooling data acquisition in their turbine reacting flow rig (TuRFR) using both cylinders and vanes. Problems were encountered during the investigations at both UND and OSU but most issues were overcome. Generally, the results of the investigation fundamentally supported the original hypothesis.

This section of the final report will be organized in a manner similar to the quarterly reports in that a summary of the work accomplished at UND will be presented followed by a similar summary for the work conducted at OSU.

UND RESEARCH OVERVIEW: The general goals to be accomplished at UND include; investigation of stagnation heat transfer to significantly expand the parameter range to levels of very high turbulence levels and Reynolds numbers, development of a cooling method to internally cool stagnation regions without the use of showerhead cooling, and documentation of full coverage slot and shaped hole film cooling for the accelerating region downstream from a stagnation region. The work is divided into six specific goals. The specific objectives for each goal are briefly listed below:

Six Key Goals. The six key project goals for UND briefly stated included: (1) Investigation of stagnation region heat transfer at very high Reynolds numbers and turbulence levels; (2) Investigation of the response of turbulence in the presence of a very large leading edge; (3) Investigation of the combined impact of roughness and turbulence on stagnation region heat transfer; (4) Investigation of internal cooling methods for leading edge regions; (5) Investigation of the influence of turbulence on full coverage film cooling methods for thermal protection of downstream pressure surfaces and suction surfaces; and (6) Investigation of the combined influence of roughness and turbulence on full coverage film cooling methods for downstream pressure and suction surfaces. Additionally, UND acquired deposition surfaces from OSU for their investigation of roughness effects on stagnation region heat transfer.

Approaches Used. The University of North Dakota's role in the current research collaboration with the Ohio State University was to investigate the leading edge heat transfer environment expected for large land based gas turbines and to develop methods to effectively cool this region. The general approach was to develop two large cylindrical leading edge test surfaces for measurements in a wind tunnel. The leading edge test surfaces were used for acquiring surface heat transfer and downstream film cooling measurements and to document the flow and velocity field encountered. In addition, a novel approach was developed for cooling leading edge regions and this internal cooling method was tested in UND's internal heat transfer and flow rig. A range of experimental approaches and instrumentation were engaged in the measurements. Instrumentation used in the study included standard thermocouple instrumentation and pressure tubing, hot wire anemometry and infrared surface temperature measurements. Heat transfer measurements were acquired using constant heat flux foils for surface heat transfer measurements while constant temperature measurements were engaged in acquiring heat transfer measurements for internal flows. Our planned approach for measuring heat transfer on rough surfaces included the fabrication of rough surface tiles using a mold of the scaled TuRFR deposit surface cast with high temperature epoxy.

Large-Scale Low-Speed Cascade Wind Tunnel. The approach for all key goals except for the internal heat transfer measurements (Goal 4) included testing in UND's large scale low speed cascade wind tunnel. The wind tunnel was modified by developing a rectangular test section which was used to test two large cylindrical leading edge test surfaces. A schematic of the wind tunnel facility is shown in Figure 1. The facility uses a 56 kW blower to entrain up to 6.6 m^3/s of air through 8-1 m^3/s high efficiency industrial bag filters. The filters are used to protect sensitive instrumentation, like hot wires from dust. The blower is capable of producing a static pressure rise of 20 inches water gauge (5000 Pa). The air is discharged from the blower into a two stage multi-vane diffuser used to recover pressure and distribute air across the face of a large heat exchanger. The heat exchanger system includes a recirculation pump and a 0.48 m^3 tank used to manage the temperature in the tunnel to a constant inlet

temperature. Downstream from the heat exchanger, air passes through a rectangular spool prior to the flow conditioning section. During this project the spool section was upgraded to include the addition of a mixer and flow straightener. The flow conditioning section consists of 4 nylon screens spaced at 5 cm prior to the 3.6 to 1 area ratio nozzle. This present described configuration represents the low turbulence condition used for testing in this wind tunnel.

Leading Edge Test Surfaces. The cylindrical leading edge test section consists of a 25.4 cm wide by 127 cm high rectangular spool which holds one of two leading edge test surfaces. The leading edge of the cylindrical test surfaces is in each case positioned 12.7 cm downstream from the entrance flange of the test section. A photo of the larger leading edge test surface is presented in Figure 2. The diameter of this leading edge test surface is 40.64 cm (16 inches) allowing approach flow Reynolds number of up to 500,000 to be tested. This leading edge Reynolds number is expected to be slightly higher than current values associated with the larger land based gas turbines. The test surface pictured in Figure 2 was fabricated using isocyanurate foam. The foam shape was fabricated using a precision jig machined using a numerically controlled endmill. The surface is covered with a 0.4 mm thick sheet of epoxy fiberglass (G10). Fine wire thermocouples are cast into holes on the surface of the epoxy board to determine the surface temperature. A 0.023 mm thick Inconel foil is used to generate a constant heat flux on the surface. The designs for both the larger and smaller cylindrical leading edge test surfaces are similar but the smaller surface has a leading edge diameter of 10.16 cm and the thermocouple spacing near the leading edge is much closer together.

The profile shapes for the larger and smaller cylindrical leading edge test surfaces are presented in Figure 3. Both profiles have a constant radius over the first +/- 30° of the surface. Later, the radius of the surface is smoothly and continually increased to produce a smooth accelerating velocity distribution as shown in Figure 4. Figure 4 shows the predicted velocity distribution over the smaller and larger test surfaces beginning at the stagnation point. These two profiles have a strong almost linear acceleration in the stagnation region before the acceleration slows down. These velocity profiles were developed to be consistent with flow acceleration in the near suction surface and pressure surface of a large turbine airfoil. The predicted velocity distributions are shown for conditions which simulate the 2nd highest leading edge Reynolds number for the two test surfaces. The stagnation heat transfer data were acquired over an eight to one range in approach flow Reynolds numbers nominally including 62,500, 125,000, 250,000 and 500,000 for the larger leading edge test surface and 15,625, 31,250, 62,500, and 125,000 for the smaller leading edge test surface. Film cooling distributions were acquired at the higher two conditions.

Turbulence Generation. The generation of a wide range of turbulence with a range of scales was a key variable for the stagnation region heat transfer and full coverage film cooling studies. The facility included four original turbulence conditions. These conditions included the low turbulence condition (LT) which was discussed in the wind tunnel section, a grid turbulence condition, and two aero-combustor turbulence conditions. Two smaller grid turbulence conditions were added for the stagnation region heat transfer study. The initial grid turbulence condition (GR) was generated using a square bar square mesh grid shown spaced at 6.35 (2.5 inches) apart. The centerline of the grid is placed 10 mesh lengths upstream from the position of the leading edge in the test surface. This grid produces a turbulence intensity of about 8% with an energy scale, Lu, of about 3.4 cm. Note that these turbulence conditions are tabulated in Table 1 and are quoted for the value at the leading edge plane of the test surface in the absence of the test surface. The smaller grid turbulence is generated in a manner similar to the larger grid. The smaller grid is constructed from 0.635 cm (0.25 inch) square aluminum bars which are spaced at 3.175 cm (1.25 inches) apart. When the small grid was placed 10 mesh lengths upstream from the leading edge it was considered to be in the close position (SG1) and it generated turbulence with an intensity of about 7.9% with an energy scale of about 1.9 cm. When the small grid was placed 32 mesh lengths upstream from the leading edge plane it was considered to be in the far position (SG2) and it generated a turbulence intensity of about 3.5% with an energy scale of about 3.3 cm. In addition to the grid turbulence, two levels of aero-combustor turbulence were generated. A schematic of the turbulence generator is presented in Figure 6. The cross-sectional view shows the inlet of the generator on the right. The flow is forced through a back panel with slots to produce a wall jet and side panels with plunged

holes to help create a recirculation zone within the mock aero-combustor liner. The flow then contracts through a two to one contraction. When this mock aero-combustor turbulence generator is placed directly in contact with the test section (AC) it produces a turbulence intensity of about 12.7% at the leading edge plane of the test surface with an energy scale of 7.2 cm. A second level of mock combustor turbulence intensity is generated when a 36 inch long rectangular decay spool is placed between the combustor simulator and the test section. This aero-combustor with spool condition (ACS) produces a turbulence intensity of around 9% with an energy scale of about 9.1 cm. During the course of this project two attempts were made to develop a very high turbulence aero-combustor. However, this will be discussed in a later section.

Response of Turbulence Near the Leading Edge. Turbulence measurements in the flow approaching the leading edge of the test surfaces were proposed to help develop a better understanding of the response of turbulence in this region. Hunt [1] predicted that in the vicinity of the stagnation region relatively small scale turbulence (with respect to the leading edge) would be intensified by the strain field while large scale turbulence would be attenuated by the leading edge surface similar to the approach flow. Britter, Hunt and Mumford [2] helped to experimentally verify the accuracy of this hypothesis. However, their work was at much lower Reynolds numbers and lower turbulence intensisties than the present work. In order to investigate this response for the present turbulence conditions in the flow fields approaching the larger and smaller leading edge test sections, turbulence measurements were acquired along the stagnation streamline of the flow. A probe traversing system was integrated into the two leading edge test surfaces as shown in Figure 7 with the flow going from left to right. However, prior to determining the response of turbulence in the leading edge region, the decay of all the turbulence conditions was determined without the test surfaces in place. Figure 8 shows a photo of the traversing mechanism which was used to document the turbulence condition along the stagnation streamline without the presence of the leading edge test surfaces. There measurements were acquired with a single wire hot wire probe at nominal inlet velocities of 5 m/s, 10 m/s, and 20 m/s. The turbulence intensity, scale, and local dissipation rate were determined from these measurements. The measurements were acquired with both the smaller and larger leading edge test surface present as well as without the test surfaces present in the test section. At high turbulence levels single wire measurements are known to be affected by lateral turbulent fluctuations, especially as the velocity decreases. Along the stagnation streamline the decrease in velocity is predictable, especially in the close proximity to the leading edge surface. However, measurements of turbulent dissipation are expected to be isotropic so these measurements are expected to provide a more accurate determination of the intensification process.

Boundary Layers Near the Leading Edge. Boundary layers developing near the leading edge were also surveyed to provide a better understanding of turbulent transport across boundary layer developing in the vicinity of the leading edge. Figure 9 shows a photo of the boundary layer probe which is being held by a traverse which was mounted inside the larger leading edge test surface. The boundary layer traverse was positioned at 30° from the stagnation line to allow the velocity over the surface to increase to high enough levels to reduce the measurement uncertainty of the velocity. The velocity profile can be analyzed to estimate the near wall shear stress. The shear stress is know to fall off with Y in an accelerating boundary layer. The fall off of shear stress is estimated from a Thomas and Hasani [3] type correlation or preferably from a laminar boundary layer calculation which includes a good estimate of the eddy diffusivity due to external turbulence. Taking the total shear stress locally and subtracting off the laminar portion, the apparent turbulent shear stress can be estimated. The turbulent shear stress estimate can in turn be used to estimate the local eddy diffusivity due to turbulence. This estimate of the local eddy diffusivity was expected to provide some insight into the intensification process imposed by the turbulence on the boundary layer.

Internal Cooling Measurements. UND uses a relatively simple internal heat transfer and flow rig for internal cooling measurements. A schematic of the facility is presented in Figure 10. The facility is powered by a pressure blower capable of flowing about 250 CFM of air at a static pressure rise of about 22 inches watergage. The 2 kW motor for the pressure blower is controlled using a variable frequency drive. The temperature of the flow can be controlled by a small heat exchanger which is integrated into

the discharge box of the blower. A 6-inch diameter PVC pipe connects to the discharge box and directs the flow through a sharp-edged orifice tube for flow measurements. Downstream from the orifice tube the flow enters a diffuser and then a flow conditioning section before connecting to the plenum of the heat transfer section. The heat transfer section plenum slowly directs the flow over the surface of the internal cooling model at shown in Figure 11. The inlet total pressure for the flow entering the cooling array is referenced from pressure taps attached to the plenum top. Two type K thermocouples are also used to monitor the inlet temperature into the plenum. The internal cooling rig can control up to 14 voltage controlled DC power supplies to power the heaters used in the cooling array. The heater voltage and current are also monitored by the data acquisition system. The current measurements uses a series of calibrated constantan shunt resisters. The pressures are monitored using a custom pressure scanner which uses two Rosemount smart pressure transmitters in parallel with 250 Pa and 5000 Pa ranges. Thermocouples are read through a passive constant temperature junction box using an HP3497A with integral voltmeter. The constant temperature junction box was referenced to an icebath.

The three geometries tested during the course of the internal cooling studies are shown in Figures 12a-12c. The geometry pictured in Figure 12a is considered the baseline geometry and it consists of a row of 11-1.27 cm diameter impingement holes, eight rows of staggered round pedestals and then a straight section which is about 1.25 diameters in length. The impingement section and the eight rows are powered by two serpentine heaters arranged in parallel. The exit sections, top and bottom, have their own individual heaters. The temperature of each section is monitored by three thermocouples on the bottom and two thermocouple on top. Each row is separated by a 0.3175 cm wide groove which is filled with a low conductivity epoxy. The top plate is adhered to the bottom plate using some high thermal conductivity epoxy over the tops of the pedestals and the top surface of the bottom edge.

The second geometry pictured in Figure 12b is one of two incremental impingement geometries. This geometry is configured to add cooling air through impingement jets incrementally along the surface to keep the coolant air temperature and resulting heat transfer level relatively constant. The impingement occurs in a cutout region behind three of the pedestals in each row. The initial impingement occurs through 6-1.058 cm holes positioned between slightly elongated pedestals in row 1. Subsequently, impingement air is added behind rows 2, 4, 6, and 8 with 3-1.058 cm diameter holes. The thermal barrier grooves and instrumentation plan is otherwise similar to the based line cooling array. The third geometry shown in Figure 12c is similar to the other incremental impingement geometry. However, the third geometry has a 0.749 cm impingement hole behind each of the pedestals in rows 2, 4, 6 and 8.

Slot Film Cooling Measurements. Assuming leading edge regions can be cooled internally, the cooling air must be discharged somewhere along the downstream pressure and suction surfaces. This film cooling air will offer thermal protection to the downstream surface as well as protection from deposition according to Prenter et al. [4]. The ideal method to discharge film cooling air is through a slot. Slots are typically not considered for turbine airfoil film cooling due to issues of structural integrity. However, the present cooling methods use double wall construction with high solidity pin arrays. High solidity arrays can reduce thermal gradients across the double wall, by providing paths to enhance thermal conduction and at the same time transmit stress. Unfortunately, this downstream film discharge would be expected to occur in regions of high acceleration and relatively high but variable turbulence. Additionally, the high solidity pin fin arrays which are used to conduct thermal energy and transmit stress are expected to produce relatively high levels of turbulence and unsteadiness within the cooling arrays. Consequently, these features need to be present inside the film cooling plenums.

The film cooling delivery system consisted of a pressure blower, a window air-conditioning unit, a thermal capacitance system, a bypass valve, an orifice tube, and a flexible hose to connect the film cooling plenum. A photo of this film cooling delivery system is presented in Figure 13. The system typically could deliver air in the 0° to 5° C range. However, some heat up occurred through the remainder of the system before discharge. The film cooling tests typically were provided a free-stream to coolant temperature difference of 10° to 12° C.

The slot film cooling insert for the larger of two leading edge test surfaces is presented in a wire frame in Figure 14a. The flow enters through a PVC pipe with 9 1.27 cm diameter lateral holes. The

cooling flow is directed through two sets of three rows of staggered high solidity pins prior to entering a collection area of 1.25 pin diameters. The plenum flow is subsequently directed into a 0.363 cm high slot slanted at 30° from the surface. The coolant exit temperature is measured with three fine wire type K thermocouples just prior to discharge. The film cooling insert is attached to the test surface using a bracket. A portion of the bracket is located at the trailing edge of the discharge slot and it contains three surface thermocouples used for adiabatic film cooling measurements and two static pressure taps. The bracket is aligned with the curvature of the test surface. The bracket integrates the G10 board which covers the test surface and it has a relieved location which holds the bus bar of the heat transfer foil. The G10 board has 60 thermocouples cast into its surface located along midspan of the surface and at +/- 5.08 cm. The test surface is fabricated from polyisocyanurate foam and it used to acquire both the adiabatic film cooling effectiveness and the downstream surface heat transfer distributions downstream from the slot.

The slot film cooling insert for the smaller cylindrical leading edge (D = 0.1016 m) test surface is presented as a wire frame in Figure 14b. The smaller leading edge film cooling plenum has a similar design to the larger leading edge. However this design has two sections of two staggered rows in the plenum. The bracket that holds the insert has a similar configuration and holds similar instrumentation as the larger insert bracket. The bracket for the smaller insert is pictured in Figure 15 as a solid model on the left and as a wireframe on the right. The G10 board is attached to the lip of the upper bracket and the indentation accommodates the heater foil buss bar. The completed slot with instrumented heat transfer foil is shown in Figure 16. The bracket with its thermocouples can be seen adjacent to the leading edge insert in the red color. The foil and its buss bar cover a portion of the bracket lip to the left of the visible section of the bracket shown in red. The location of where the air enters the plenum can be seen at the top surface of the test section.

Full Coverage Shaped Hole Film Cooling. A full coveraged array of shaped holes was also tested on the larger leading edge film cooled test surface. The tests were conducted over the same Reynolds numbers and coolant flow rates as the slot film cooling occurred at. The full coverage array of shaped holes consisted of two rows of holes which were staggered. A wire frame schematic of the leading edge film cooling insert geometry is presented in Figure 17. The plenum is very similar to the larger slot film cooling plenum. However, in order to accommodate the array of film cooling holes only a total of five rows of high solidity pin fins were added to the feed channel of the film cooling holes. The hole arrangement is presented schematically in Figure 18. The holes have a spanwise pitch of three diameters as well as a streamwise pitch of 3 diameters. The holes were set at a 30° incline to the surface. The shaped holes expand laterally at an angle of 8° to ensure there is no separation inside the film cooling holes and also to produce better coverage. The wall thickness was set at twice the hole diameter which was 5.59 cm. When the centerline of the hole crossed the surface plane the discharge hole was approximately 2.1 times the round hole area. The hole array included 12 upstream holes and 13 downstream rows. A direct view into the holes is shown in Figure 19. Three fine wire thermocouples were installed near the exit of three of the holes. The film cooling measurements were conducted on the same heat transfer surface as the slot film cooling measurements. The integration of the shaped hole insert with the film cooling and heat transfer test surface is pictured in Figure 20. At the lowest two turbulence levels some spanwise variation in the film cooling was expected downstream of the array of discrete shaped holes. Consequently, the test surface was painted black and dots of low IR emissivity paint were located on the surface in order to enable the mapping surface locations. A full surface visualization of the downstream film cooling effectiveness for the shaped hole array is presented in Figure 21. The test was run at an approach flow Reynolds number of 250,000 at a blowing ratio of 0.97, for the small grid far (SG2) condition. The figure was generated from the difference between two IR images of the surface. One was taken for an adiabatic wall case and one was taken at the blowing ratio of 0.97. The IR measurements provided a method to assess the spanwise variation of the film cooling protection.

Stagnation Region Heat Transfer Measurements at Very High Turbulence Levels. Turbulence levels at the exit of combustion systems can be very high. Turbulence levels of up to 28% have been reported in the literature (See Van Fossen and Bunker [5]). In an effort to further extent the

parameter range for stagnation heat transfer augmentation due to turbulence, a very high turbulence generator was designed and built. Photos of the first and second attempts at building this turbulence generator are pictured in Figure 22. The initial attempt was developed by scaling the turbulence generator in Figure 6 by 50%. However, this initial turbulence generator had no contraction, produced a poor velocity distribution and had a limited flow range due to a relatively small flow area. The original very high turbulence generator liner is shown on the left side of Figure 22. The newer second attempt is shown in the photo to the right. This turbulence generator is scaled to 62.5% of the original and it has a 1.25 to 1 area ratio contraction into the test section. The system has 87% of the flow area of the original liner through the use of plunged elliptical holes in the liner walls and proportionately wider slots in the back of the liner. The new very high turbulence generator's downstream velocity profile is shown in Figure 23. The profile is attached and the high turbulence quickly redistributes the flow to a very reasonable velocity distribution. The turbulence generator produces a turbulence intensity of 17.4% which is 37% higher than the older mock combustor. The turbulence generator produces a scale of around 7.2 cm.

Problems Encountered: Several problems were encountered over the course of UND's portion of the research program. The first problem encountered was overcoming the difficulty in the development of a very high turbulence generator with a good inlet velocity profile. Another problem included managing wind tunnel set point issues in conjuction with film cooling testing during warm weather. A related problem involved reducing a temperature stratification which occurs in the tunnel at the highest velocity. A final problem involved the development of a realistically rough surface using the previous procedure which UND had developed for building this type of surface.

Development of a Very High Turbulence Generator. Developing a very high turbulence generator with a good inlet velocity profile proved to be a challenging task. The initial approach was to scale the original turbulence generator, as shown in Figure 6, by 50%. This reduction in the liner to test section contraction was believed to be the best approach to develop this very high turbulence level. However, in spite of producing a very high level of turbulence the turbulence generator produced separated flow on one side of the combustor exit. In order to smooth out the downstream velocity distribution, a short rectangular spool was fabricated and attached to the turbulence generator. A grid was inserted in the short spool section to provide a uniform resistance across the flow to help smooth out the velocity distribution. The grid did inprove the velocity profile somewhat but it also reduced the turbulence level. Additionally, due to the size of the combustor inlet flow area, the resulting pressure drop was high and the upper end of the flow was limited to about 75% of the previous mock combustor. As a result of these problems, it was decided to develop a new very high turbulence generator. Figures 24 and 25 compare the exit and entrance of the older and newer aero-combustor turbulence generators. In Figure 24 the newer turbulence generator is on the right and the small thickwall plunged tubes can be seen in the inside of the turbulence generator liner. These tubes block 66% of the exit flow, which likely helps to cause the separated flow near the exit. Conversely, the older turbulence generator has a 2 to 1 area ratio contraction which undoubtably helps to alleviate any flow separation downstream from the second row of plunged holes. Figure 25 shows the entrance to the older and newer mock combustor turbulence generators on the left and on the right. The latest very high turbulence generator is discussed in the previous section and is presented in Figures 22 and 23.

Hot Day Film-Cooling Temperature Control. The temperature control of the film cooling air became a problem during warmer summer days when running the shaped hole film cooling tests. At the higher Reynolds number, the fan provides 8 times the power and 4 times the temperature rise compared with the lower Reynolds number during film cooling tests. Consequently, the wind tunnel heat exchanger was run with a significant flow rate. This kept the tunnel air temperature steady. However, the blower for the air conditioner also needed a higher pressure to feed the film cooling air. This resulted in a notable temperature rise across the fan. However, without a similar heat exchanger, the air temperature exiting the film cooling blower rose significantly above the tunnel air temperature. Additionally, humidity in the air caused a further load on the A/C unit causing difficulty in maintaining a good tunnel to film cooling discharge temperature difference. In order to improve the A/C cooling air temperature

control a heat exchanger along with a cooling water recirculation system was installed at the outlet of the film cooling blower as presented in Figures 26 and 27. Figure 26 pictures the new heat exchanger in its plenum box and Figure 27 shows the connection between the blower, the heat exchanger plenum and the remainder of the film cooling supply system. This upgrade to the film cooling delivery system enhanced our ability to achieve the proper film cooling test conditions across our entire test matrix range.

Wind Tunnel Temperature Stratification. UND's large scale low speed cascade wind tunnel is designed to operate from inlet velocities as low as 2.5 m/s to velocities as high as 20 m/s. Over this range of flows the power requirements for the fan increase substantially. As the blower changes from 10 m/s to 20 m/s the facility sees roughly an 8 to 1 increase in power and a 4 to 1 increase in the energy which the blower is adding to the flow. In order to keep the facility operating at steady state, the energy applied to the flow in the blower needs to be removed in the heat exchanger. At the highest velocity level for the low turbulence flows, the wind tunnel produces a stratification of temperature across the span of the wind tunnel. At the higher turbulence levels, the turbulence typically mixes out any spanwise stratification. Although this temperature stratification is typically stationary and can be subtracted if an adiabatic surface temperature distribution has been taken, if conditions change between the film cooled or heated test cases and the adiabatic test cases, this temperature variation can lead to an error. With the use if infrared thermography with shaped hole film cooling measurements, it was believed that the stratification might result in a problem. Consequently, a preconditioning section mixer and flow straightener was designed, fabricated and installed. This cross span mixer was installed just downstream from the heat exchanger in the rectangular section connecting the heat exchanger to the wind tunnel flow conditioning section as pictured in Figure 28. The mixer on the left is designed to enhance mixing between the two sides of the flow path downstream from the heat exchanger. Subsequently, the flow is reconditioned in a flow straightener shown on the right in Figure 28. This mixer effectively reduced the temperature stratification and improving the spanwise temperature uniformity in the flow.

Realistically Rough Surface Modeling. One significant problem encountered during the present project was the development of a realistically rough surface based on surfaces generated by OSU's TuRFR. The surface selected for modeling is represented as a 3D visualization in Figure 29. Previously, this type of surface was modeled by fitting a series of element heights as a function of distance using a spline fit. Then the entire surface was modeled as a surface by knitting all the lines together in the solid modeling package. Initially some of the spline fits failed due to rather abrupt changes in the surface geometry. These failures were "fixed" by smoothing out a few points in the line. However, in spite of a number of iterations like this, the surface could not be developed. Later, the individual lines were expanded by adding points from the spline fit in between other points. However, this change still did not work. UND expected to overcome these difficulties but this aspect of the project was initiated too late and we were not successful. If an opportunity to model and fabricate these surfaces presents itself in the future, we are interested in pursuing the heat transfer and film cooling measurements with this roughened surface.

Changes to Original Methodology: There were no significant changes to the original methodology.

Impact of Project Results: The project had a number of significant impacts in areas related to turbine cooling. The project impact areas include: stagnation region heat transfer, the response of turbulence in a stagnation region, internal cooling for leading edge regions, and downstream film cooling using both slots and arrays of shaped holes. In the area of stagnation region heat transfer we developed two very large cylindrical leading edge test surfaces. The combination of these surfaces along with the six different turbulence conditions developed with the wind tunnel enabled the significant expansion of the turbulence intensity, Reynolds number, length scale to diameter Reynolds number range. These data, presented in Figure 30, demonstrated that the rate of increase in augmentation levels decreased with an increasing TRL parameter. This work is important because it helps to improve predictions for the very large leading edge regions that are being designed for the largest land based gas turbines. Previously, there was no data in

the literature which supported heat transfer predictions in the stagnation region for these large gas turbines.

The Response of Turbulence. Turbulence measurements were also taken in the approach flow along the stagnation streamline of the larger and smaller leading edge test surface as well as without the surface. These data provided some very useful understanding of the response of turbulence in the presence of the larger and smaller leading edge test surface. One of the clearest indications of the response of turbulence was the elevation of the dissipation rate in the leading edge approach flow as shown in Figure 31. Several issues were uncovered by the investigation. First, the data showed very little intensification of the relatively large scale turbulence (AC & ACS) in the presence of the smaller leading edge. Next, the data suggested that turbulence with larger time scales generally experienced higher levels of intensification than turbulence with smaller times scales. Finally, the data indicated that the increased convection time caused by the large leading edge region had a significant influence in causing increased decay for smaller time scale turbulence (Lu/u').

Boundary Layers. Boundary layer measurements were taken at a location of about 30° on the larger leading edge (D = 0.4064 m) test surface. The boundary layers were acquired in a region of high acceleration. The nominal shape factor was 2.2 for all boundary layers. The boundary layers helped to document the approach flow for the film cooling. Additionally, the boundary layers were analyzed to estimate the eddy diffusivity distributions. Generally, the near wall eddy diffusivity distributions were consistent with the ATM model of Ames et al. [6].

Incremental Impingement. A new internal cooling method call incremental impingement was developed during the course of the project to enable the internal cooling of leading edge regions. Leading edge regions are typically cooled with showerhead film cooling. However, showerhead cooling can be disruptive to boundary layers [7] and showerhead cooling holes are locations where deposition can find a foothold [8]. This new method combines a high solidity double wall cooling array with impingement set in cavities behind pedestals to continually replenish cooling air along an array in an effort to manage the local heat load. The cooling capacity of conventional cooling arrays falls off as the coolant absorbs the external heat load. However, as shown in Figure 32, incremental impingement keeps heat load levels high across an array and provides high levels of cooling near the exit region. Incremental impingement offers an effective and efficient cooling method for leading edge regions which is deposition tolerant. Spent air from incremental impingement can be effectively used for downstream thermal protection.

Slot Film Cooling. Webb et al. [8] notes that showerhead and downstream film cooling holes can be preferential sites where deposition can form. However, Prenter et al. [4] suggests that slot film cooling can offer a significant level of protection for surfaces against deposition. At UND an effort was made to develop a useful database for slot film cooling in situations similar to what might be encountered on the downstream pressure surface or near suction surface after incremental impingement. This comprehensive slot film cooling database was developed over six turbulence conditions, four blowing ratios, two Reynolds numbers over two geometries. An example of this database is presented in Figure 33 which shows slot film cooling at a blowing ratio of 0.42 for the six turbulence conditions. This figure shows the dramatic influence of turbulence on downstream film cooling and suggests that the local turbulence level may be the key variable in determining the downstream film cooling distribution.

Full Coverage Shaped Hole Film Cooling. Double wall cooling arrays with high solidity pins are designed to overcome the structural integrity challenges imposed by slots. However, some cooling configurations may be better served using a full coverage array of shaped holes. Figure 34 presents shaped hole film cooling data at a blowing ratio of 0.54 with four turbulence levels comparing data at higher and lower Reynolds numbers. The film cooling data can be seen to be much better at the lower Reynolds number. This difference is attributed to the transitional nature of the boundary layer at the lower Reynolds number. Transitional behavior is common in the highly accelerating regions of vanes. The data also show the very significant impact of the turbulence on these full coverage shaped hole array film cooling distributions. Further, it is interesting to note that the downstream effectiveness levels are similar at the higher and lower Reynolds numbers.

Stagnation Region Heat Transfer. One of the goals of the project has been to develop a very high turbulence level simulated combustor to further expand the stagnation region heat transfer parameter range. Towards the end of the project the second very high turbulence generator was completed and tested and it was used to document the influence of this very high turbulence on stagnation region heat transfer. This new turbulence generator increased the available turbulence level by 37% from around 12.7% to around 17.4% with a comparable scale. This enabled the expansion of the TRL parameter by 38%. The resulting Nu/Nu0 versus TRL distribution is presented in Figure 35. Most importantly these data show the slope of the heat transfer augmentation at this very high turbulence condition and it should bracket the TRL range encountered by the modern large scale land based gas turbines.

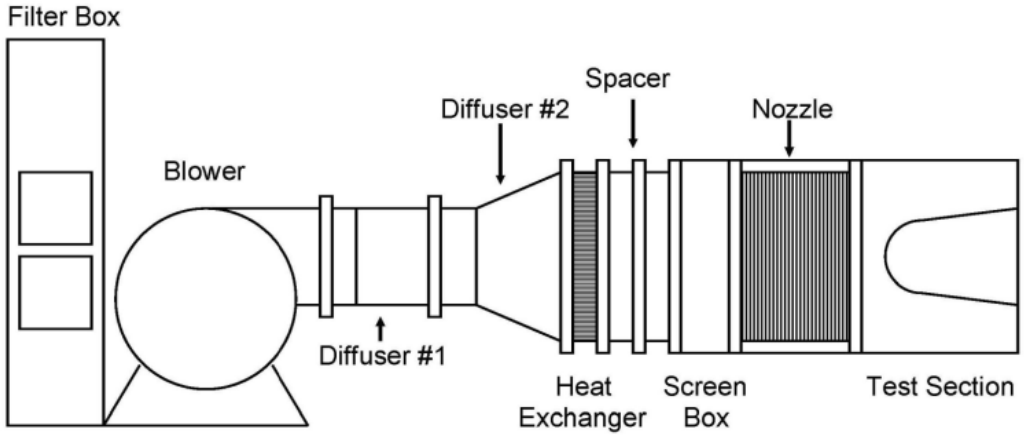

Figure 1. Wind tunnel facility used for stagnation heat transfer experiments.

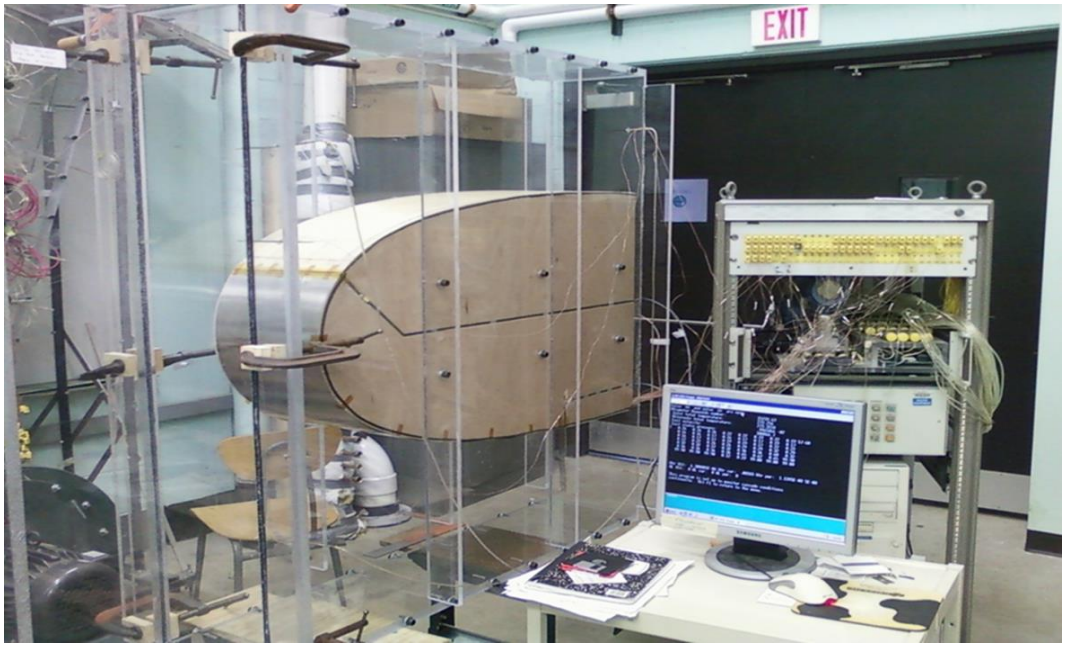

Figure 2. Photo of large cylindrical leading edge test surface installed in wind tunnel test section

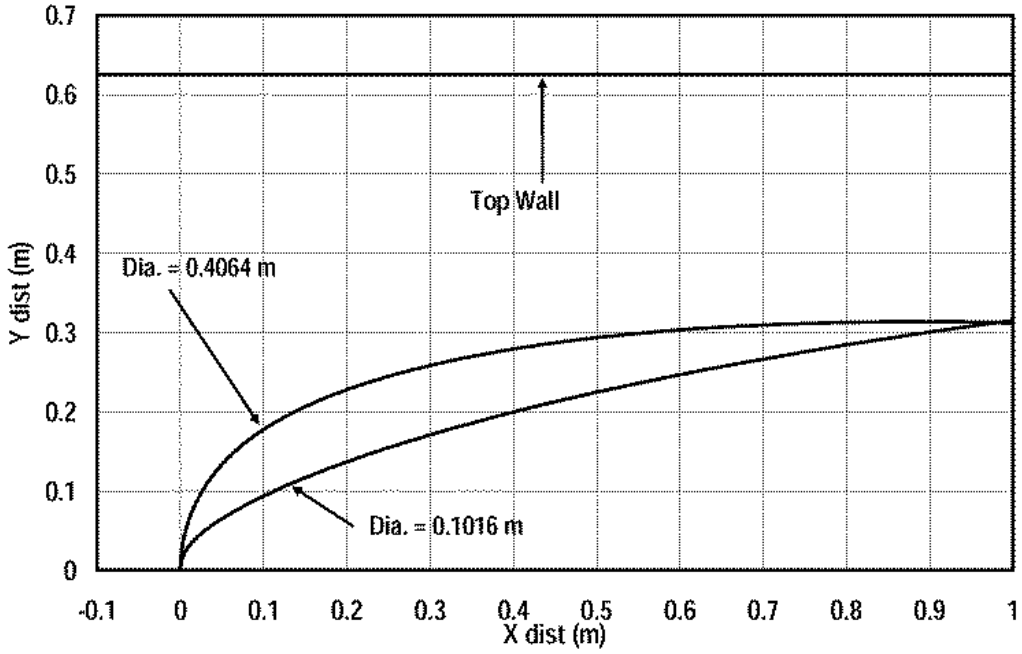

Figure 3. Half profiles of smaller and larger cylindrical leading edge test surfaces with top wall.

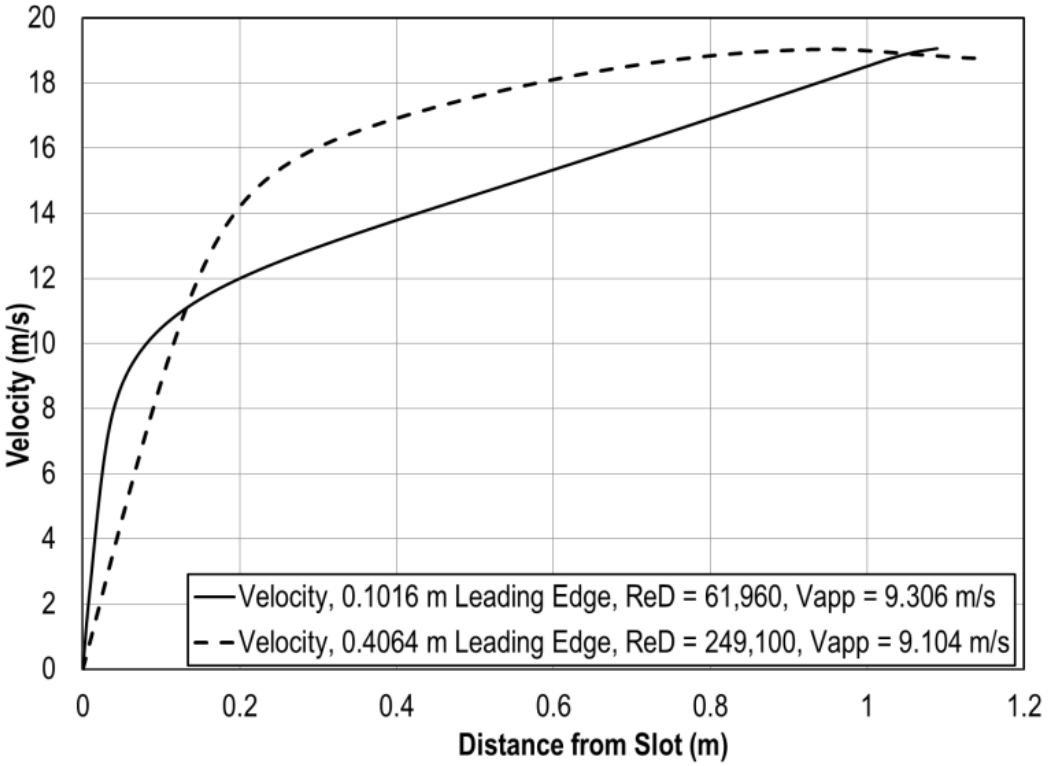

Figure 4. Surface velocity distribution for smaller and larger leading edge test surface.

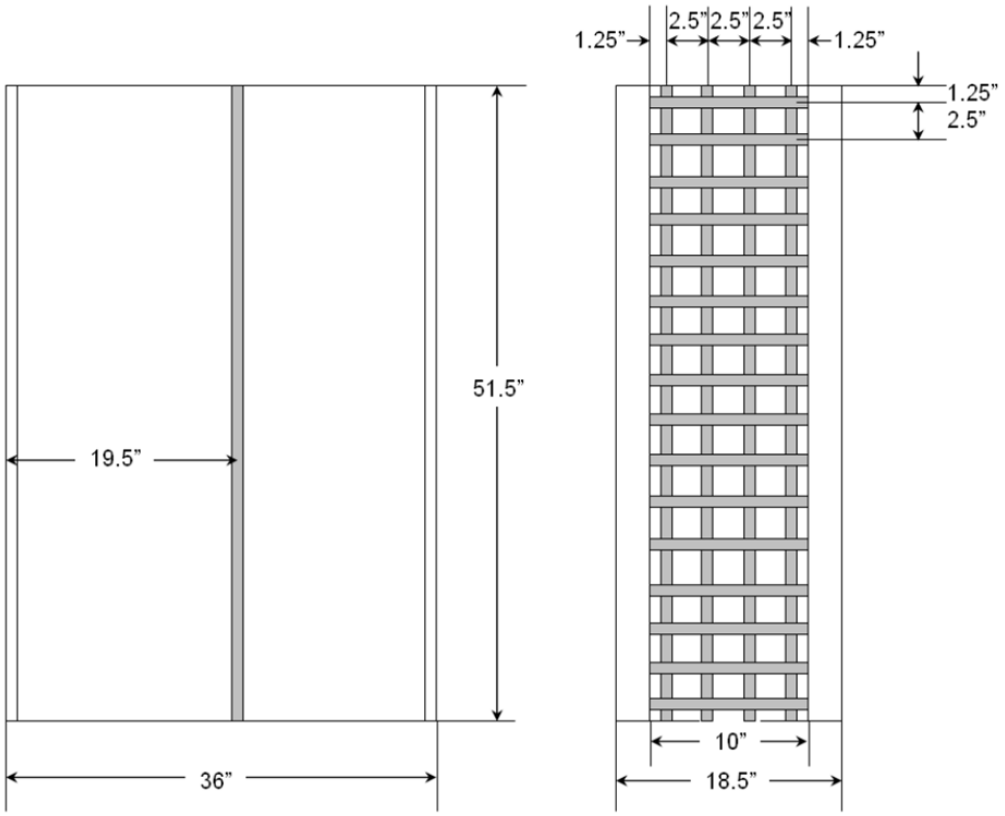

Figure 5. Schematic of larger square bar (1.27 cm) square mesh (6.35 cm) grid set 10 mesh lengths upstream from the leading edge.

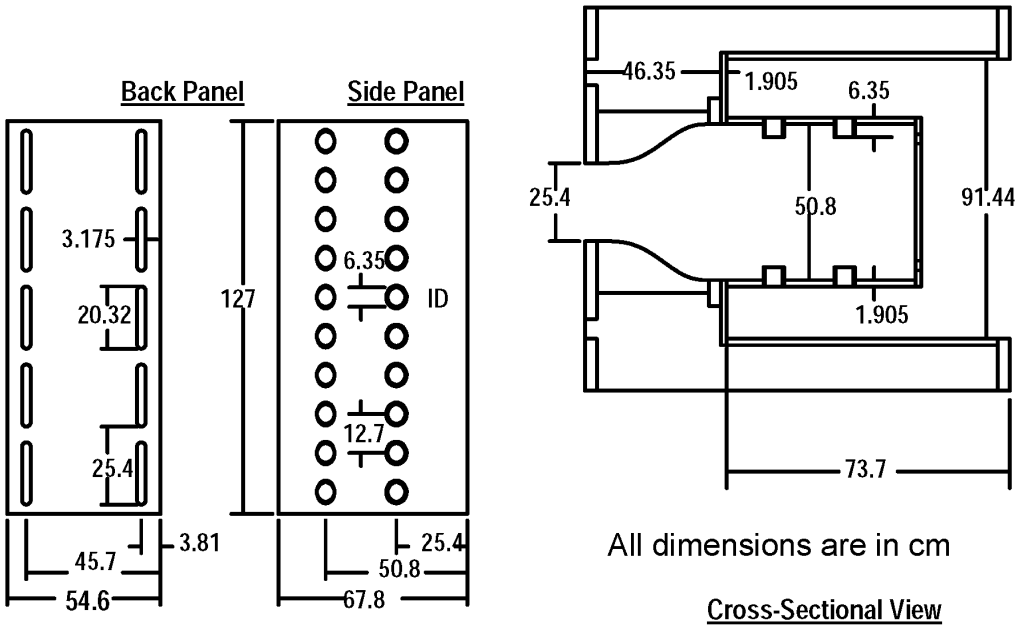

Figure 6. Schematic of original aero-combustor turbulence generator cross-section showing back panel slots for wall jets and side panel plunged holes for primary and dilution holes.

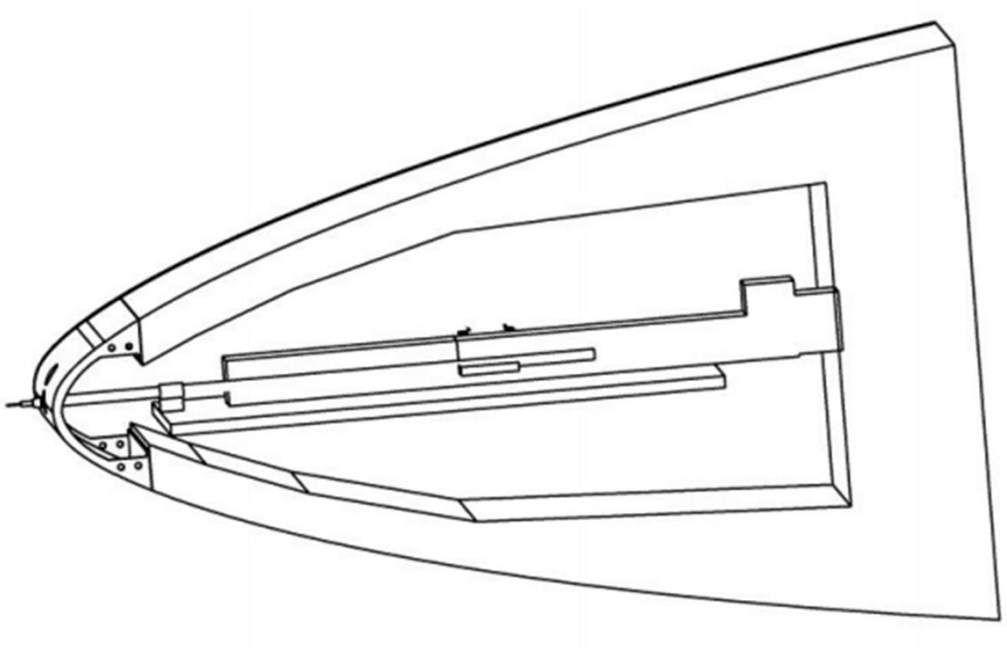

Figure 7. Schematic of 0.1016 m (4”) cylindrical leading edge test surface with stagnation stream line traverse installed.

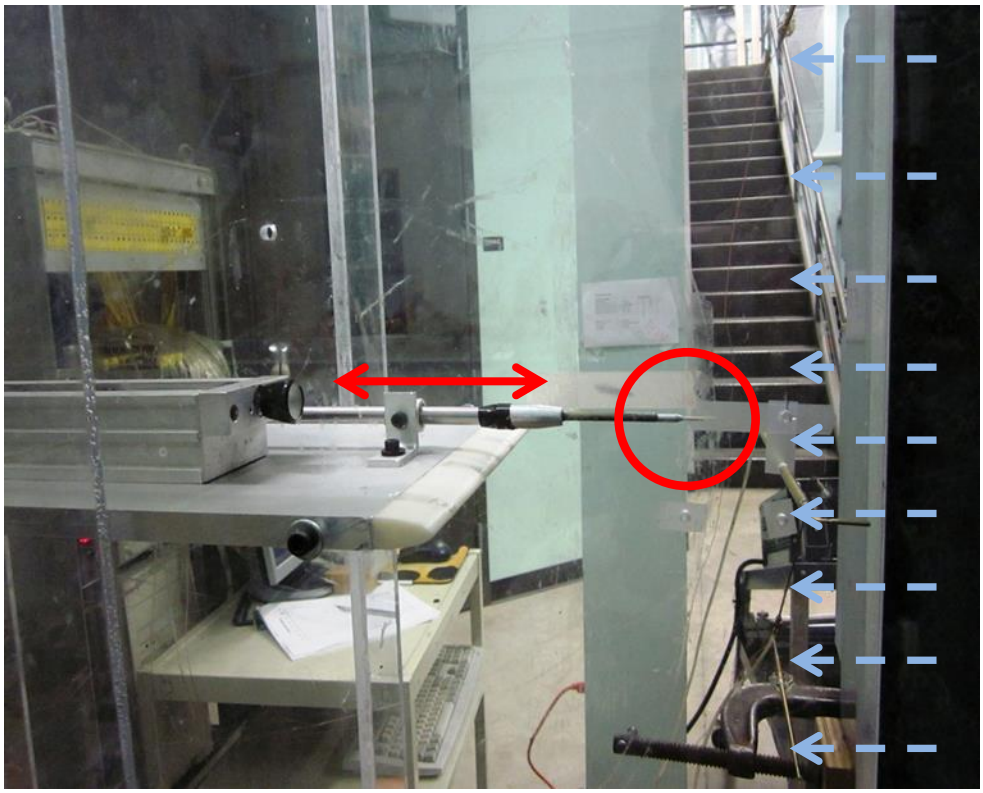

Figure 8. Photo of traversing section inside the testing tunnel.

Figure 9. Photo of boundary layer traverse mounted inside large leading edge test surface.

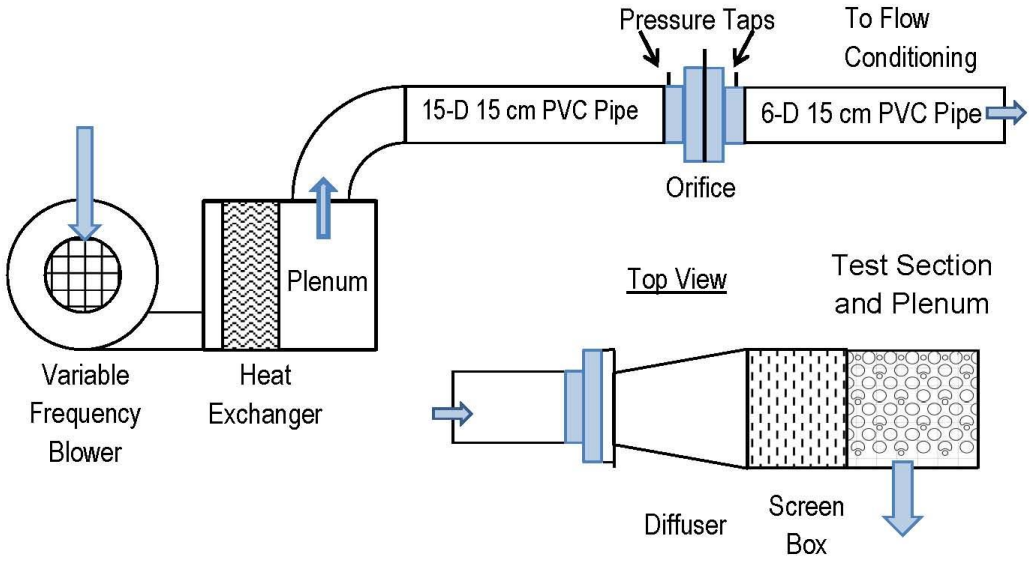

Figure 10. Schematic of internal cooling array heat transfer and flow rig.

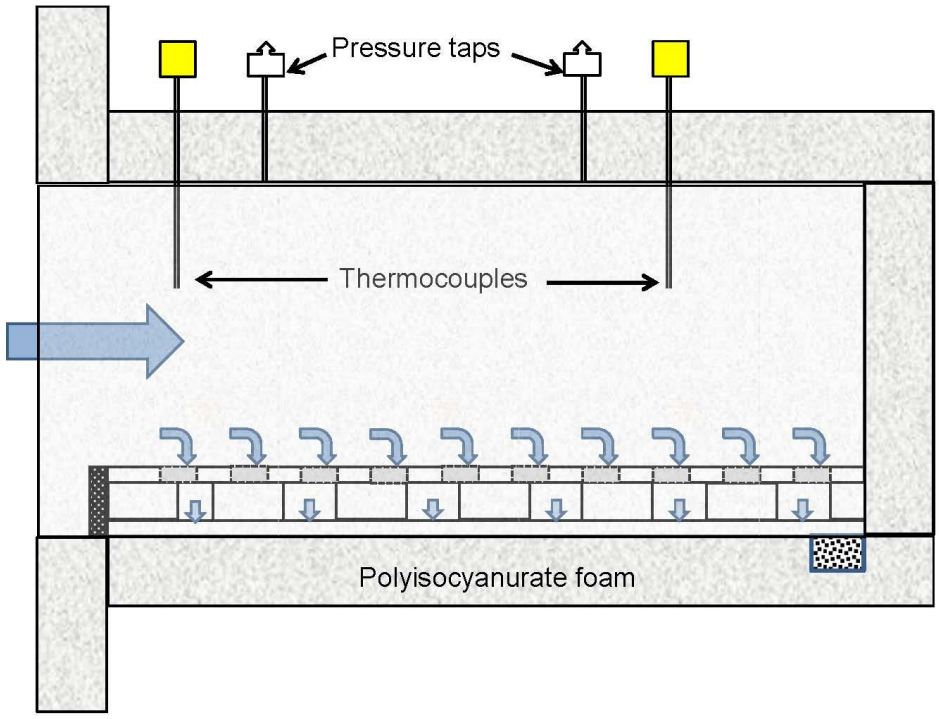

Figure 11. Schematic of side view of heat transfer rig plenum with cooling array installed.

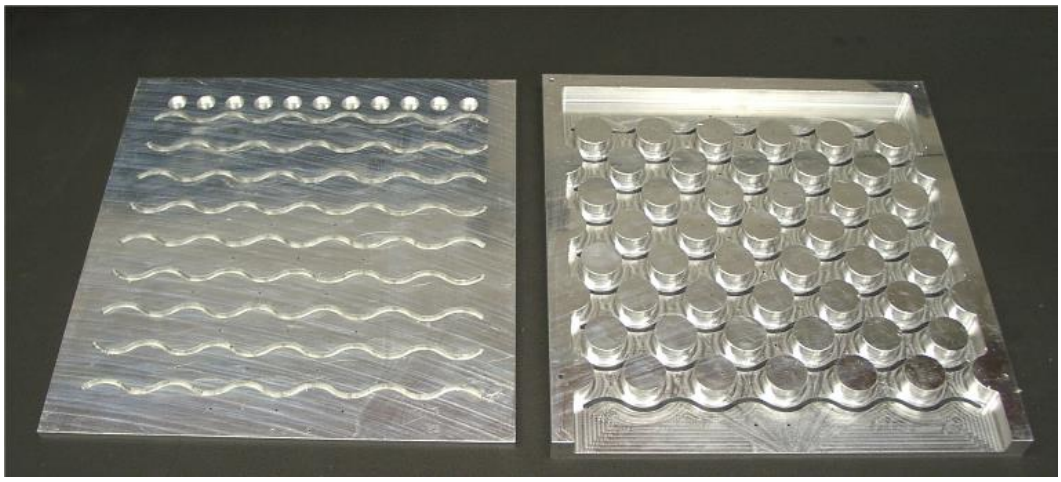

Figure 12a. Photo of top and bottom surfaces for high solidity pin fin array with inlet impingement holes.

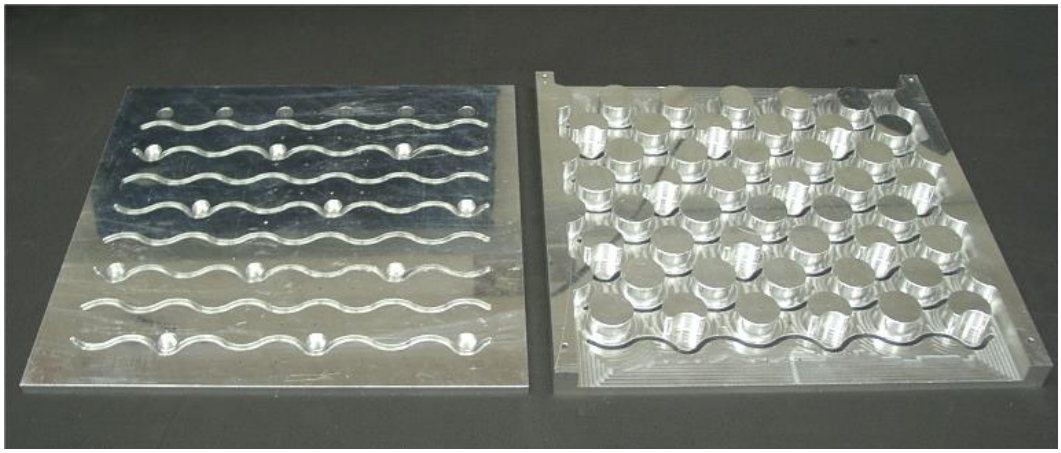

Figure 12b. Phto of top and bottom plates for initial configuration for incremental impingement high solidity pin array.

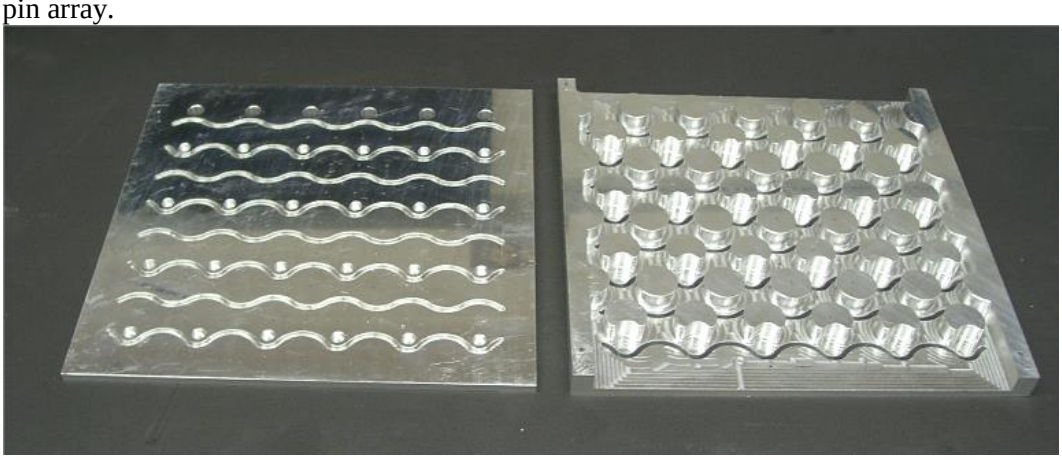

Figure 12c. Photo of top and bottom plates for second incremental impingement array with high solidity pin fins.

Figure 13. Film Cooling Air Delivery System Showing Blower, AC Unit, Thermal Capacitance Unit and Orifice Tube.

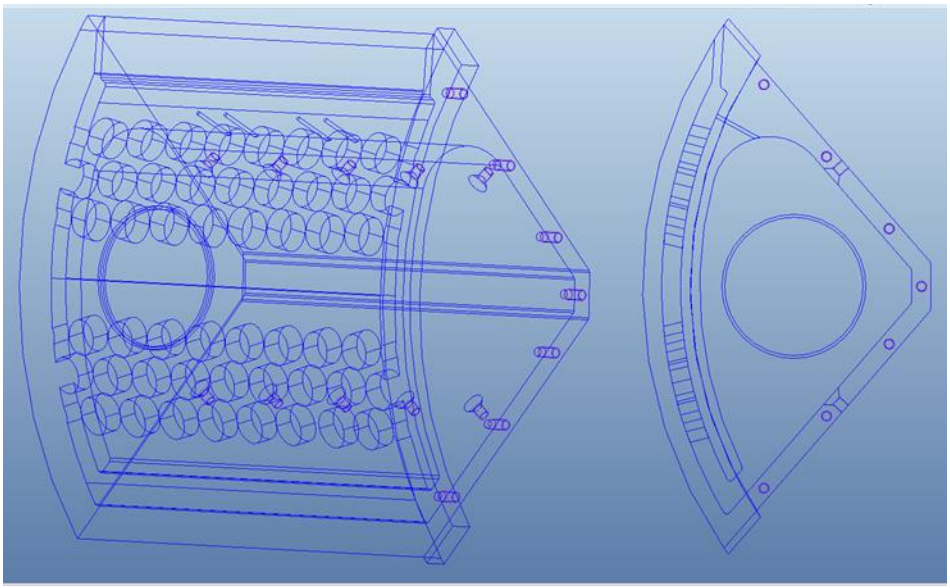

Figure 14a. Schematic of slot film cooling insert for larger (0.4064 m) cylindrical leading edge test section.

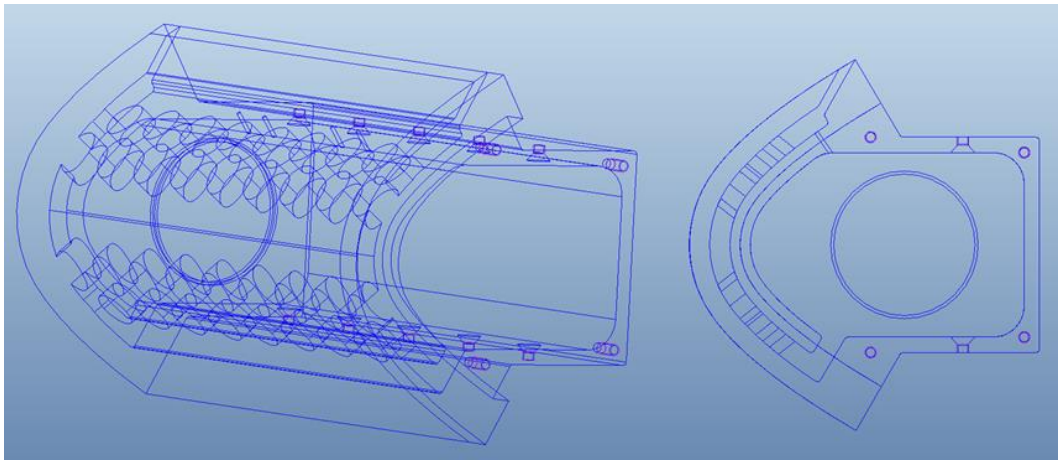

Figure 14b. Schematic of slot film cooling insert for smaller (0.1016 m) cylindrical leading edge test section.

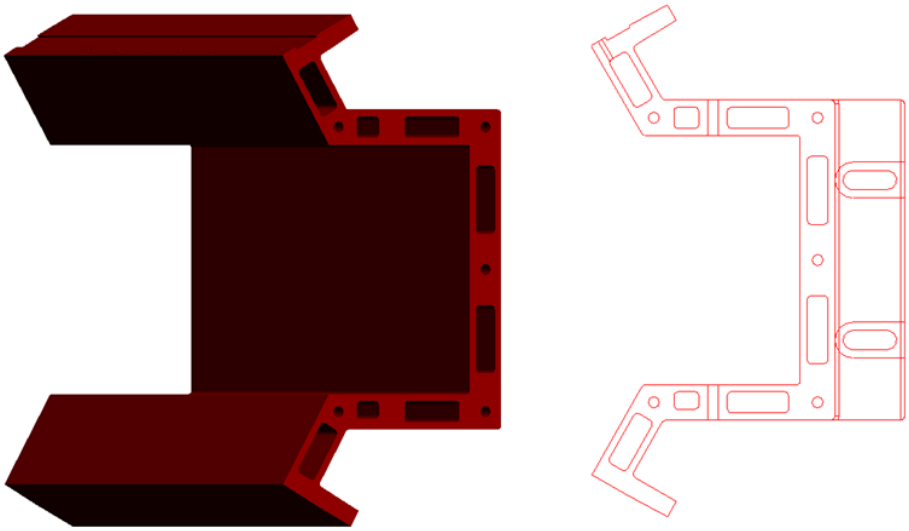

Figure 15. Solid model and wire frame model of leading edge support bracket for smaller diameter film cooled insert.

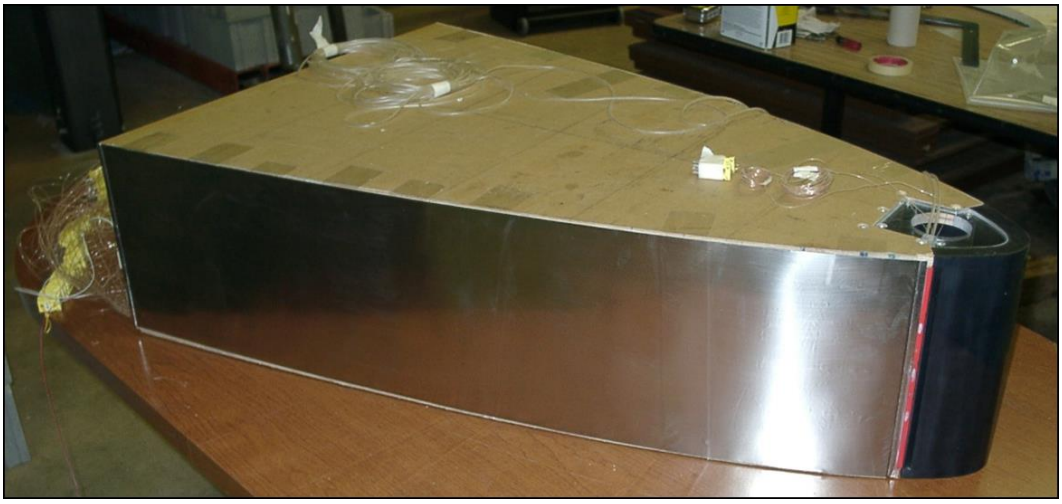

Figure 16. Photo of smaller film cooling cylindrical leading edge test surface.

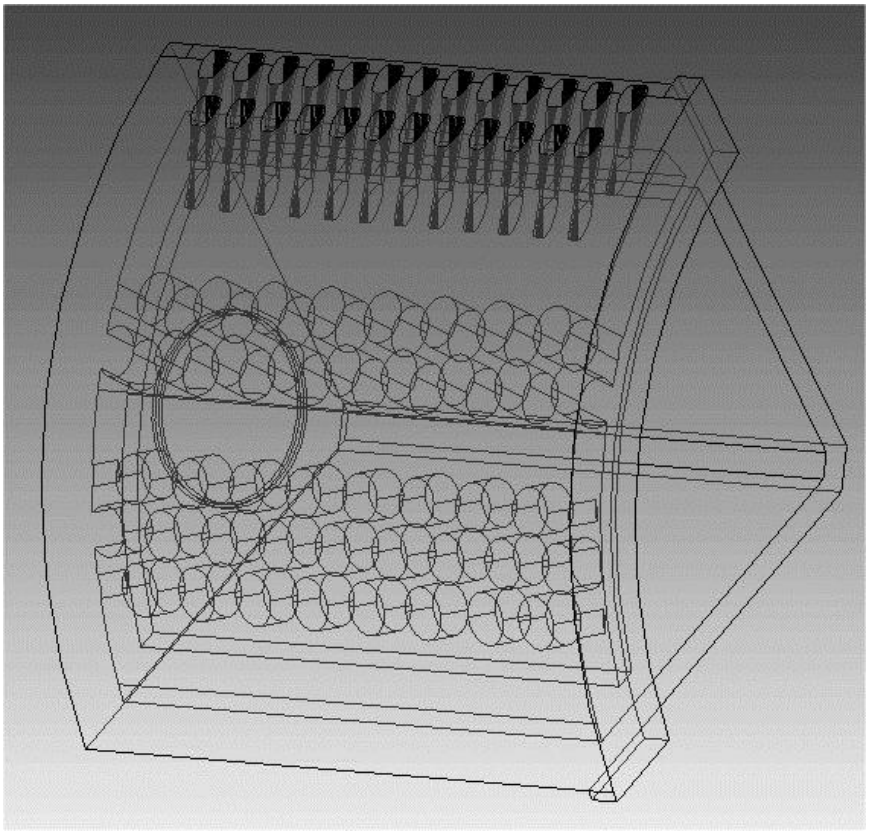

Figure 17. Schematic of shaped hole film cooling insert for large cylindrical leading edge test surface.

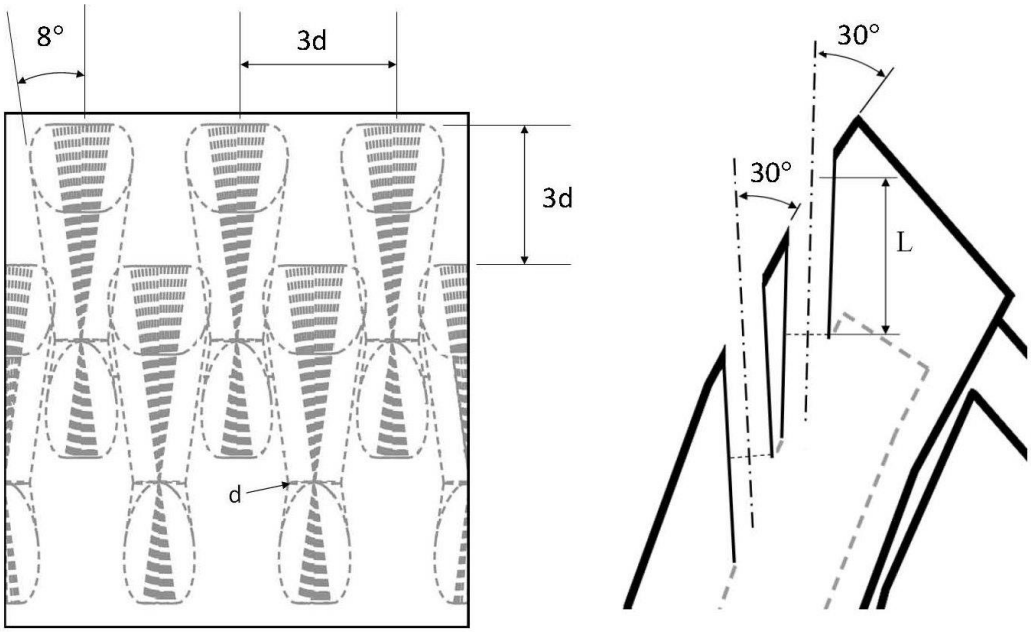

Figure 18. Schematic of shaped hole array and shaped holes as configured for the leading edge film cooling insert.

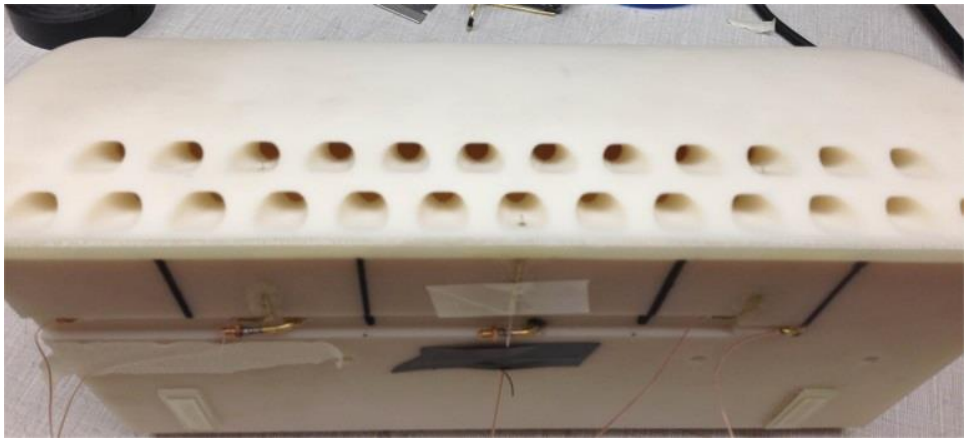

Figure 19. Photo of shaped hole insert showing full coverage staggered array with intra-hole thermocouples.

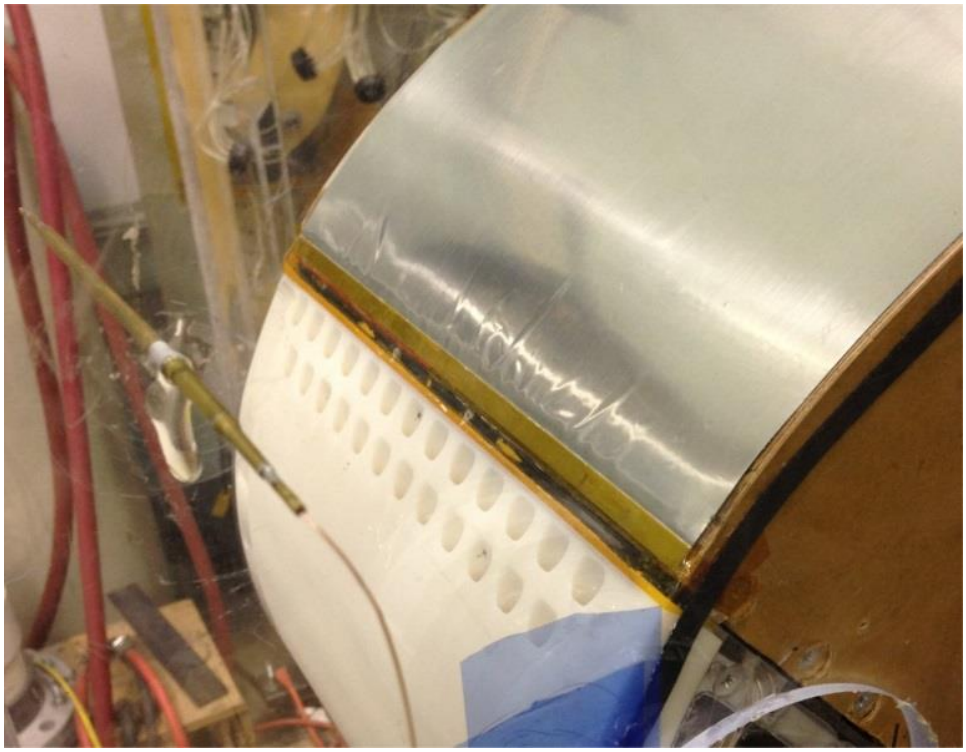

Figure 20. Photo of shaped hole insert installed onto cylinder upstream of bracket instrumentation and heat transfer foil.

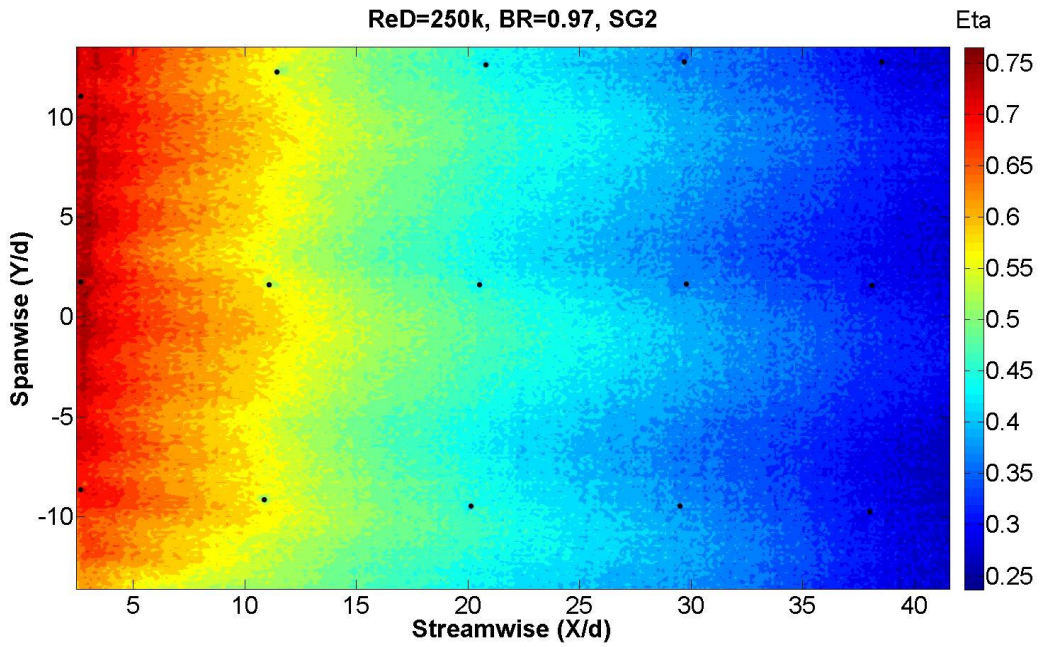

Figure 21. Full surface, IR, film cooling visualization, M = 0.97 small grid near (SG2) showing spanwise variation of film cooling effectiveness.

Figure 22. Comparison of old and new very high turbulence aero-combustor simulator.

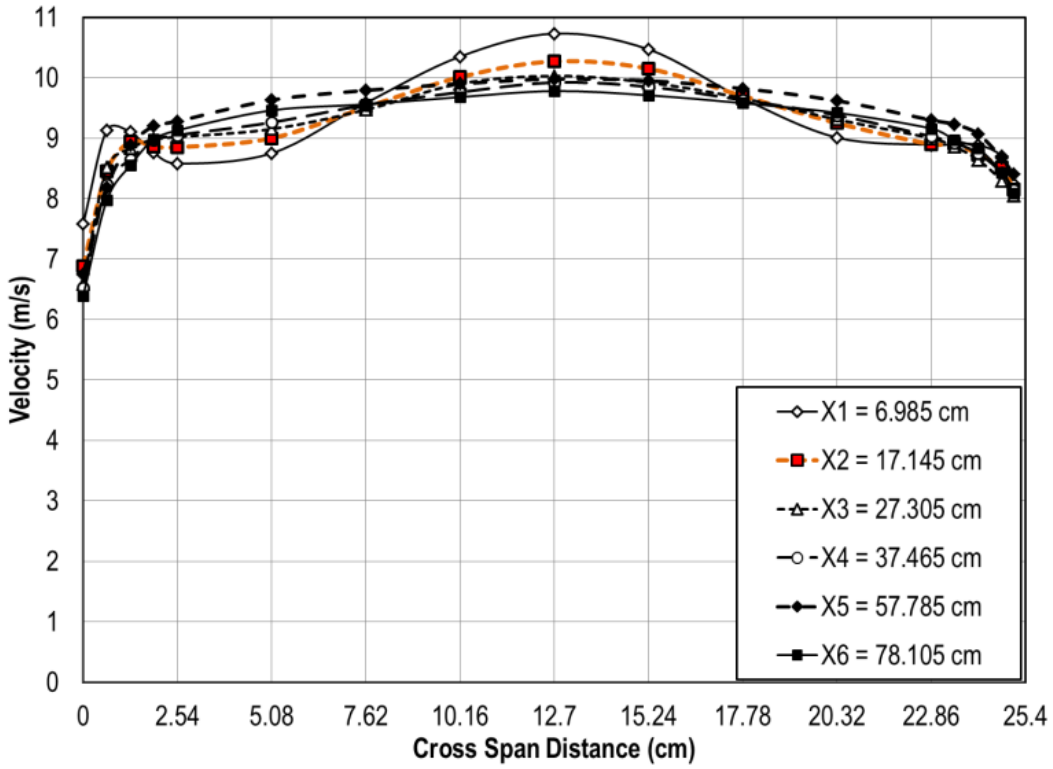

Figure 23. Cross-span velocity distributions at various distances downstream from turbulence generator.

Figure 24. Front view of Aero Combustor and High Turbulence Generator.

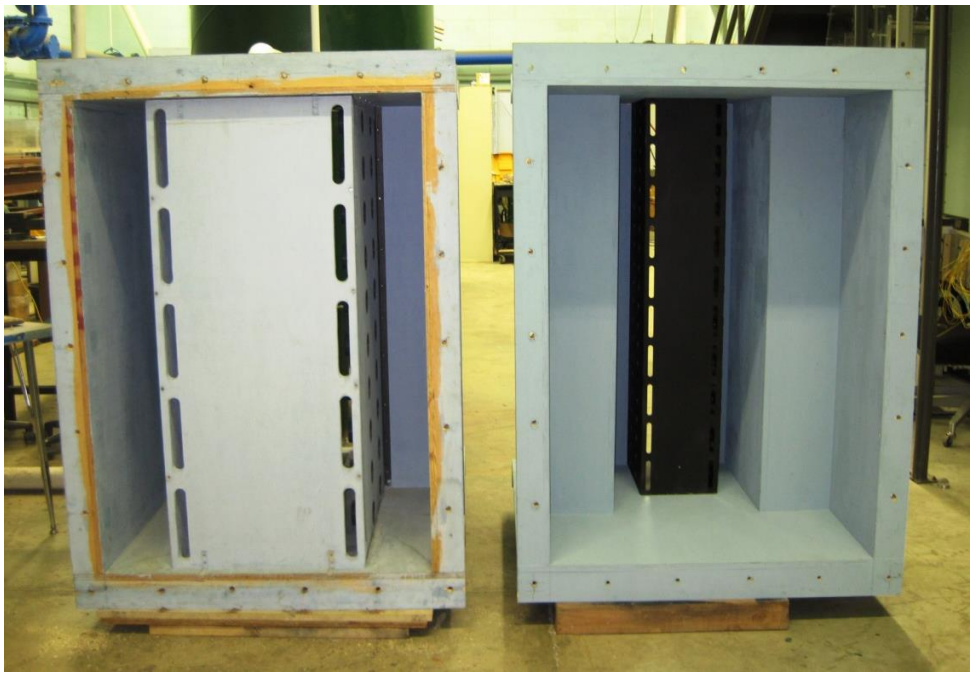

Figure 25. Rear view of Aero Combustor and High Turbulence Generator.

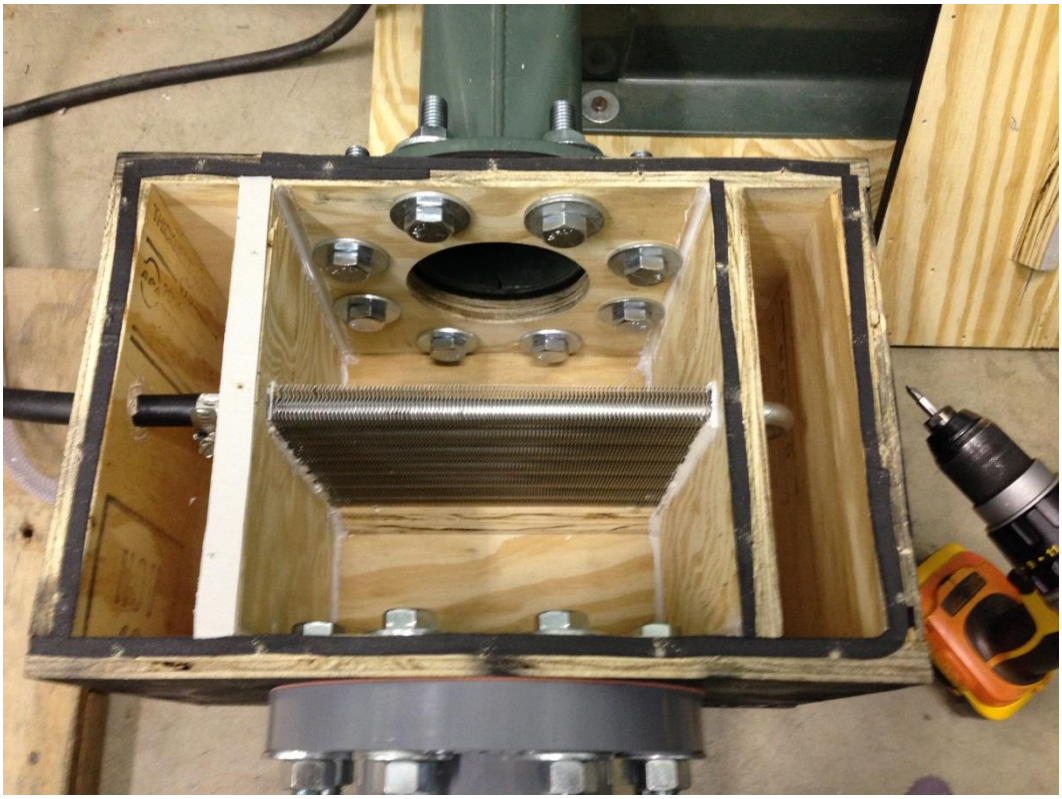

Figure 26. Picture of film cooling air heat exchanger for heat transfer air temperature control.

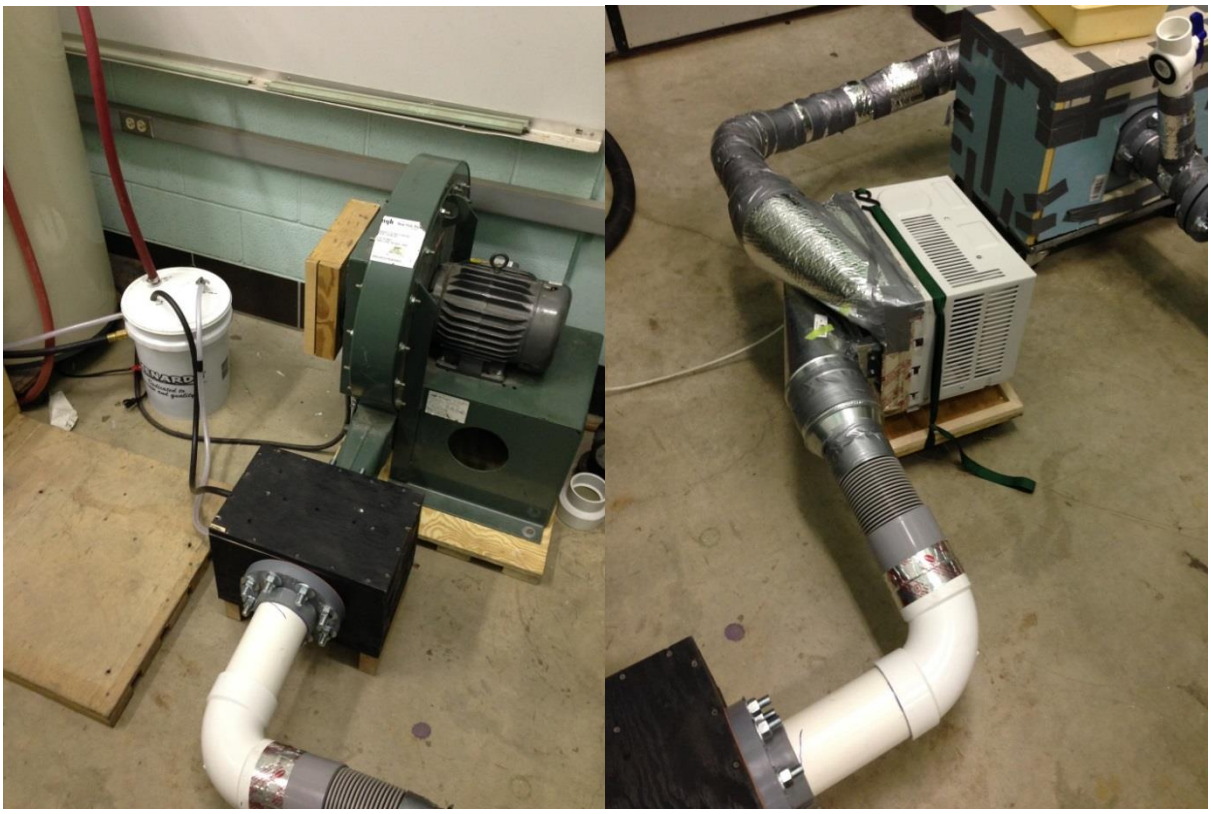

Figure 27. Photos of heat exchanger and recirculation system installed in film cooling air system.

Figure 28. Photos of flow mixer and flow straightener installed in wind tunnel inlet duct.

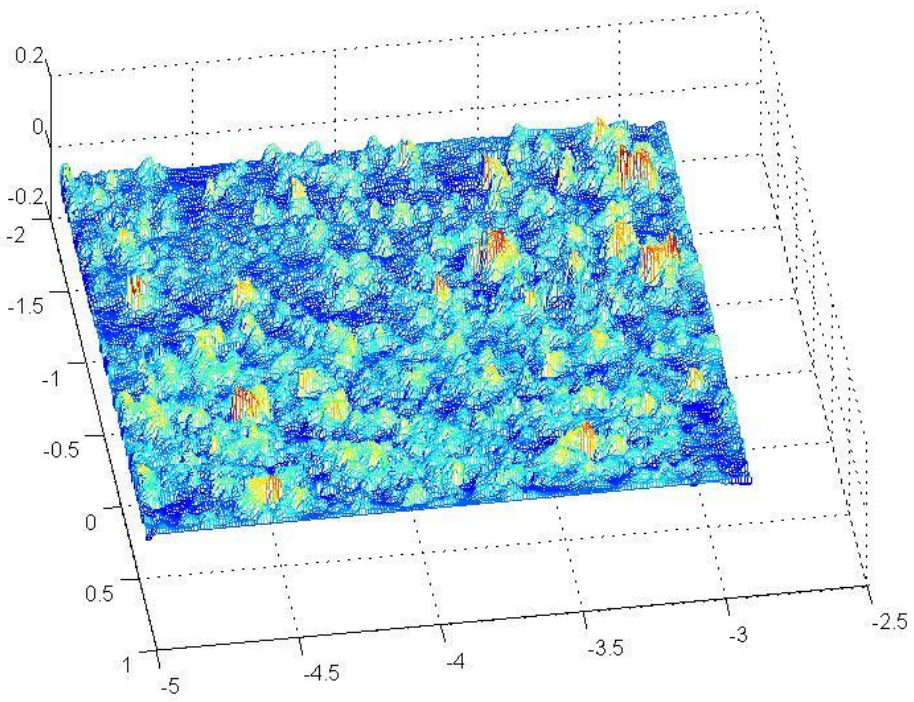

Figure 29. Visualization of scaled roughness surface for application to leading edge test surface.

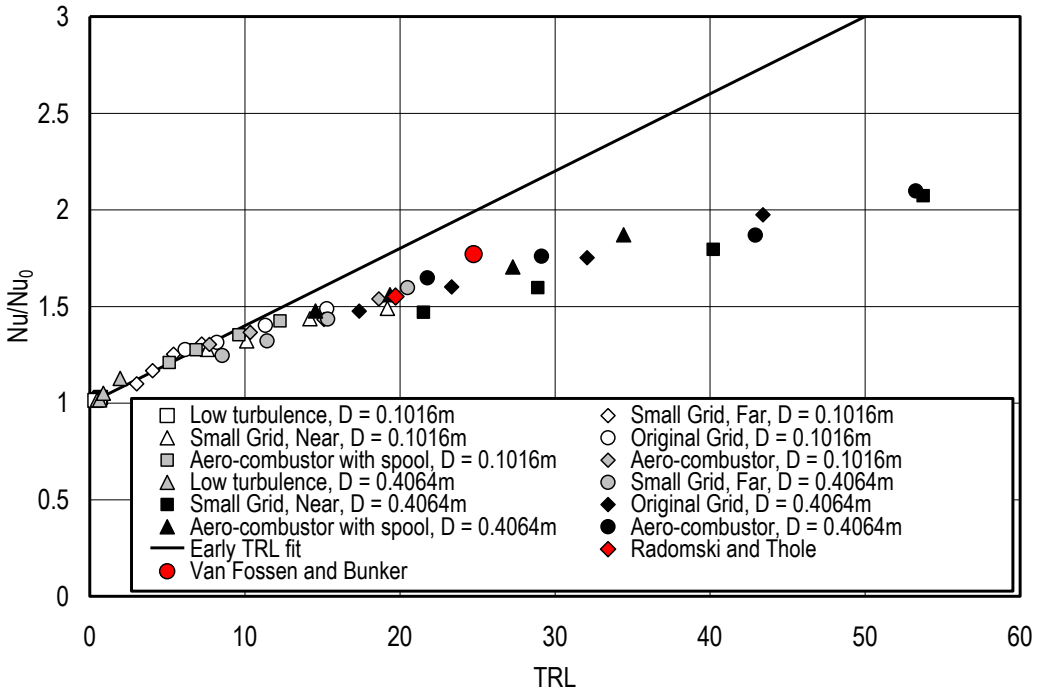

Figure 30. Nusselt number versus TRL parameter for medium and large cylindrical leading edge test surfaces.

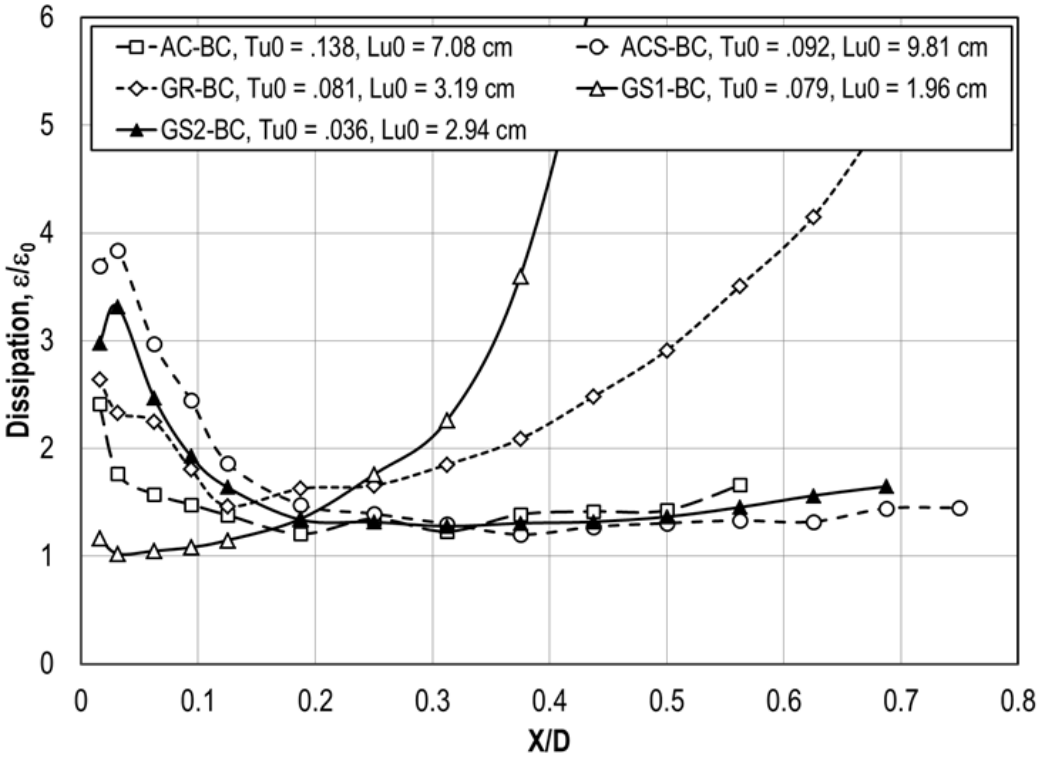

Figure 31. Streamwise distribution of normalized dissipation, $\varepsilon/\varepsilon_0$, in approach flow, 0.4064 m diameter leading edge.

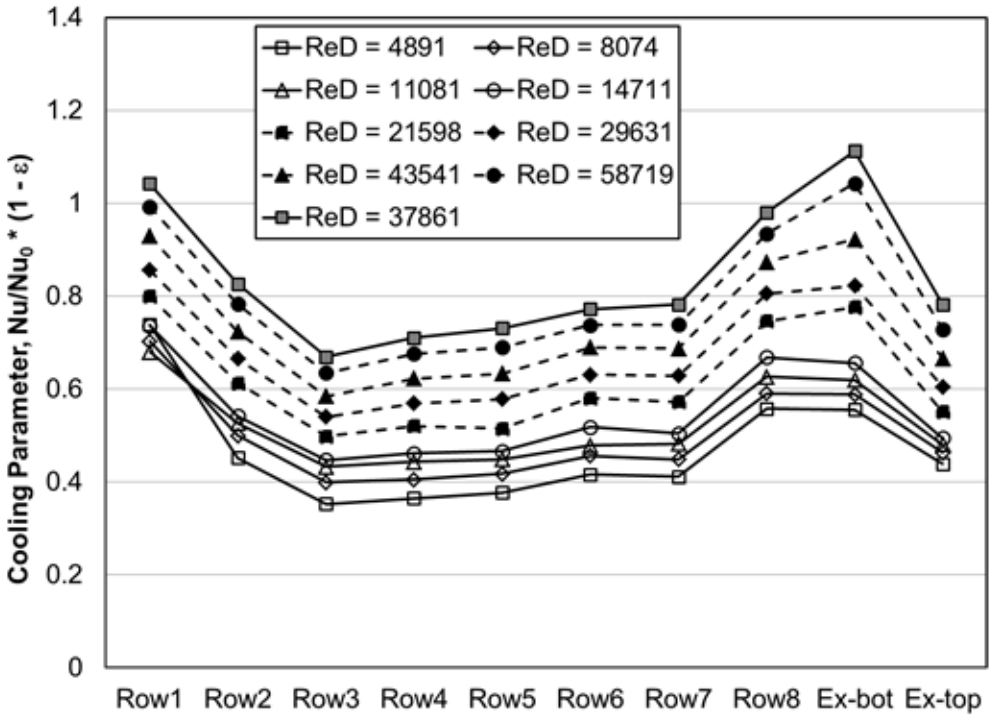

Figure 32. Cooling parameter as a function of row location and Reynolds number for cooling configuration 1.

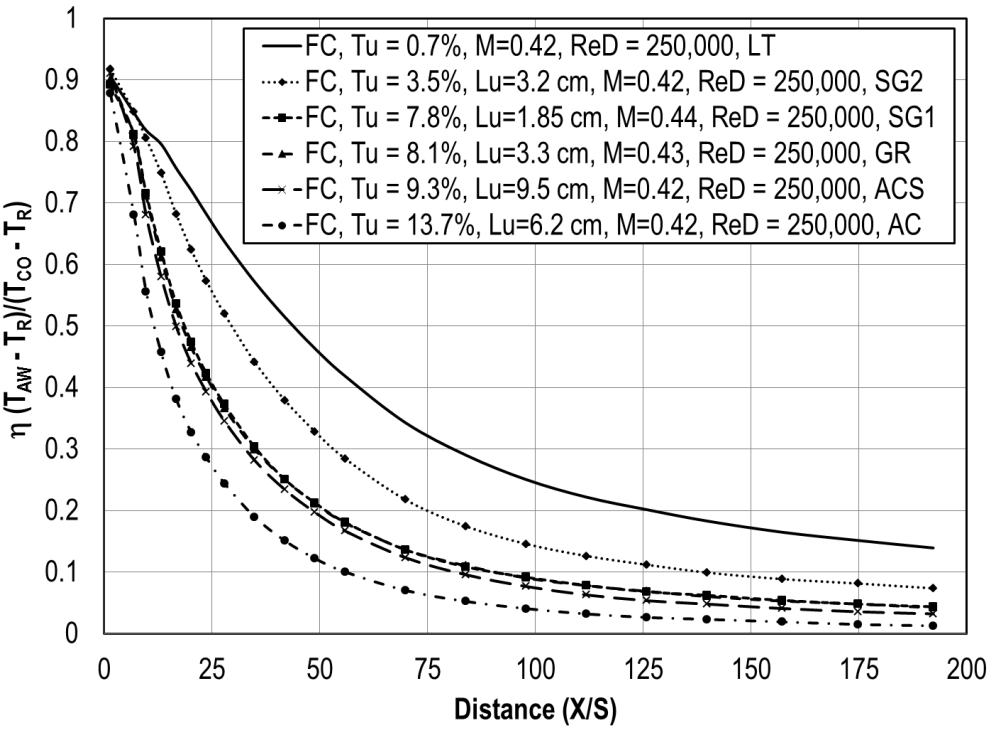

Figure 33. Adiabatic film cooling effectiveness, M = 0.42, variable turbulence condition, larger cylinder, Re_D = 250,000.

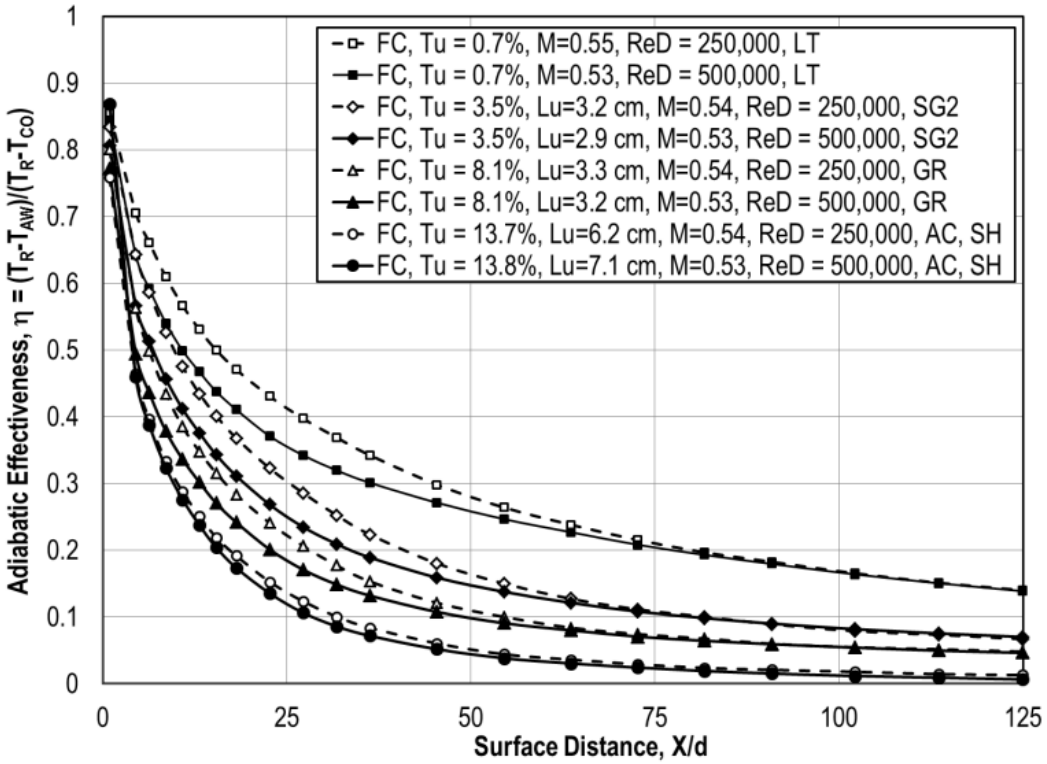

Figure 34. Adiabatic film cooling effectiveness, M = 0.54 comparing shaped holes turbulence conditions and Reynolds numbers.

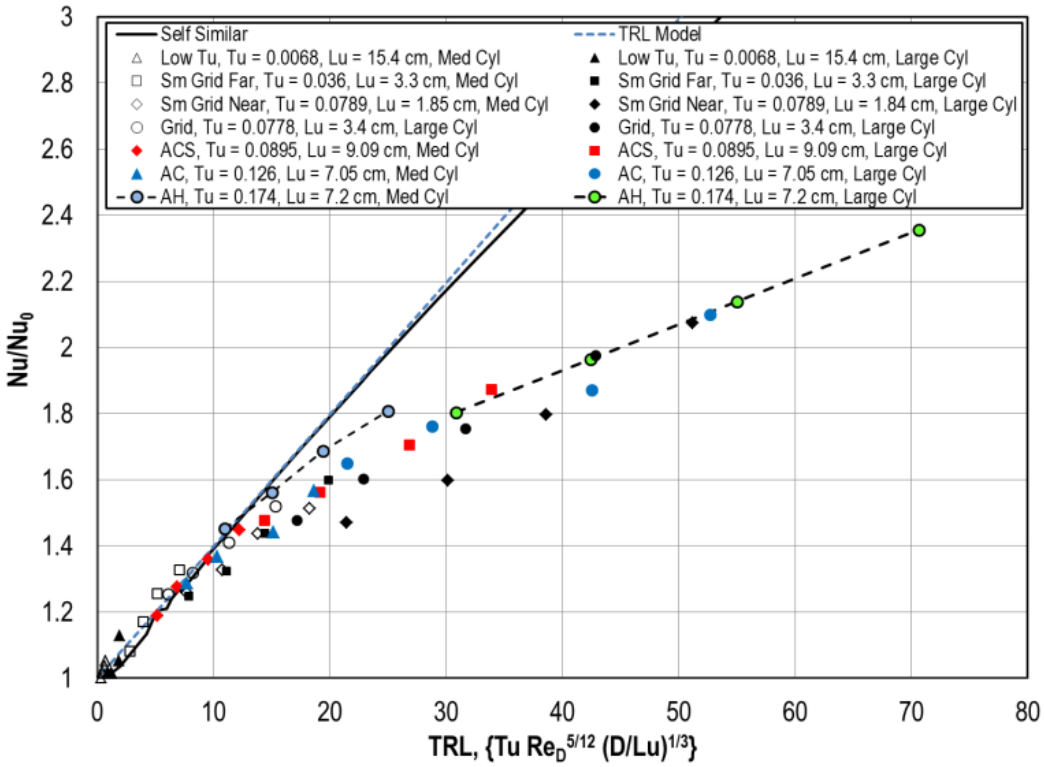

Figure 35. Expanded stagnation heat transfer results with very high turbulence generator (AH).

Table 1. List of turbulence conditions generated for current UTSR research study at UND.

	U (m/s)	Tu	Lx (cm)	Lu (cm)	ε (m^2/s^3)
AH	4.89	0.1744	3.76	6.66	13.95
	9.72	0.1744	3.91	7.22	101.3
	19.34	0.1718	4.00	7.69	715.9
AC	4.84	0.1235	3.68	7.24	5.61
	9.11	0.1302	3.52	6.36	42.1
	18.11	0.1259	3.58	7.35	253.4
ACS	4.84	0.0883	5.08	9.03	1.53
	9.17	0.0916	4.61	8.81	12.06
	17.60	0.0897	4.44	9.49	68.63
GR	4.93	0.0755	2.00	3.27	2.13
	9.94	0.0790	2.04	3.35	23.4
	18.95	0.0813	2.35	3.53	163.4
SG1	4.48	0.0808	1.51	1.78	4.00
	9.12	0.0781	1.61	1.85	29.4
	17.87	0.0792	1.12	1.97	216.0
SG2	4.70	0.0384	2.38	3.81	0.232
	9.08	0.0350	1.73	3.23	1.49
	17.61	0.0348	2.13	2.85	12.1
LT	4.96	0.0069	8.12	127.0	0.00005
	9.65	0.0076	5.02	154.5	0.00038
	18.71	0.0061	3.58	15.50	0.0139

References

1. Hunt, J.C.R., 1973, "A theory of turbulent flow round two-dimensional bluff bodies," J. Fluid Mech., vol. 61, part 4, p. 625.
2. Britter, R. E., Hunt, J.C.R., and Mumford, J.C., 1979, "The distortion of turbulence by a circular cylinder," Journal of Fluid Mechanics, vol. 92.
3. Thomas, L.C., and Hasani, S.M.F., 1989, "Supplimentary Boundary-Layer Approximations for Turbulent Flow," J. Fluids Eng., **v.** 111, pp. 420.427.
4. Prenter, R., Whitaker, S.M., Ameri, A., and Bons, J.P., 2014, "The Effects Of Slot Film Cooling On Deposition On A Nozzle Guide Vane," ASME Paper No. GT2014-27171.
5. Van Fossen, G.J. and Bunker R.S., 2001, "Augmentation of stagnation region heat transfer due to turbulence from a DLN can combustor," ASME J. Turbomachinery, vol. 123, pp. 140-146.
6. Ames, F.E., Kwon, O., and Moffat, R.J., 1999, "An algebraic model for high intensity large scale turbulence," 99-GT-160.
7. Ames, F.E., 1998, "Aspects of Vane Film Cooling with High Turbulence: Part I - Heat Transfer," *ASME J. Turbomachinery,* vol. 120, pg. 768.
8. Webb, J., Casaday, B., Barker, B., Bons, J.P., Gledhill, A.D., and Padture, N.P., 2012, "Coal Ash Deposition on Nozzle Guide Vanes—Part I: Experimental Characteristics of Four Coal Ash Types," *J. Turbomach.* 135, 021033-1-9, Nov 08, 2012.

OSU RESEARCH OVERVIEW: This research effort is part of a larger grant from DOE/NETL to UND to explore the effect of free-stream turbulence level, geometry, deposition, and cooling on the heat load experienced by turbine vane leading edges. The tasks to be accomplished at OSU include; experimental deposition studies for various combinations of free-stream turbulence level, leading edge diameter, and coolant design. The work is divided into three specific phases. The specific objectives for each phase are listed below:

Phase 1. Develop a suitable test bed for deposition studies with different leading edge diameter.

5) Generate deposits on a turbine vane and on a faired cylinder stand-in. Determine if deposition mechanism is similar in LE region. Determine the conditions under which a faired cylinder is a good model for LE deposition on turbine vane.
6) Decision point:
    a. If a faired cylinder is NOT a good model – use vanes for study and seek other partners/hardware for larger LE radius vanes
    b. If a faired cylinder IS a good model – compare deposition on various LE radii cylinders at constant gas temp, inlet Mach, particulate type and loading.
7) Measure deposition rate, surface roughness, deposit thickness, and composition
8) Send deposit surfaces to UND for modeling

Phase 2. Explore influence of free-stream turbulence level on deposition

f. Since turbulent diffusion is known to be a significant mechanism for deposition in turbines, different freestream turbulence levels will be generated in the OSU TuRFR.
g. Study deposition rate for various turbulence level and leading edge diameter combinations
h. Measure deposition rate, surface roughness, deposit thickness, and composition
i. Send deposit surfaces to UND for modeling
j. Explore use of infrared camera and cylinder-integrated thermocouples to determine the heat load during deposition as well as evolution of deposition under different flow conditions.

<u>Phase 3</u>. Explore use of film cooling to mitigate deposition in the leading edge region AND on pressure surface near passage throat.

d. Various cooling patterns will be explored on faired cylinders in the TuRFR to determine their effectiveness at mitigating deposition.
e. An actual turbine vane will also be installed in the TuRFR to explore the effect of cooling on deposition in the leading edge and pressure surface region.
f. Send deposit surfaces to UND.

RESEARCH FACILITY

The OSU deposition cascade facility (Turbine Reacting Flow Rig or TuRFR) is designed with a natural gas burning combustor and metered particulate injection (Fig. 36 schematic). The facility can operate at gas temperatures up to 1200C, equivalent to F-class engine hardware. Various coal ash samples (bituminous, lignite and sub-bituminous) are used as particulate. The TuRFR accommodates the positioning of multiple passages of actual engine hardware at the combustor exit. For this project it has been redesigned to accommodate faired cylinders as substitutes for the nozzle guide vanes.

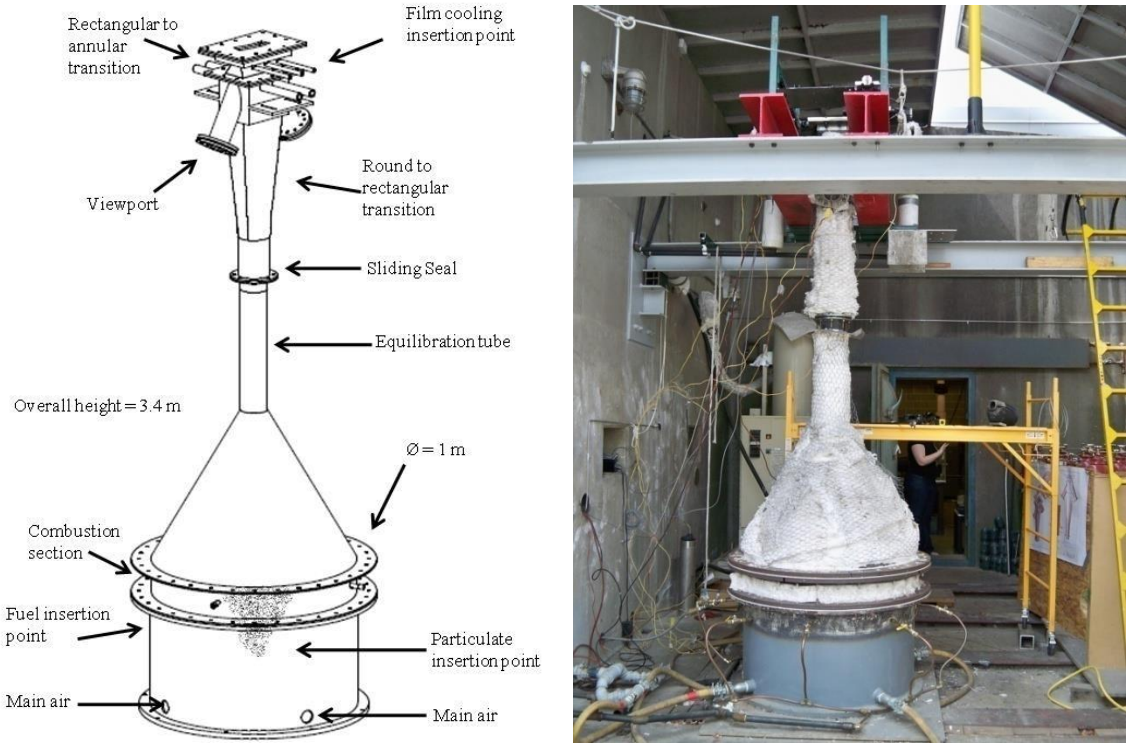

Figure 36. Schematic of the OSU Turbine Reacting Flow Facility (TuRFR).

PHASE 1 SUMMARY

The initial focus of this phase was to explore the hypothesis that faired cylinders are a suitable substitute for actual turbine vanes as pertains to leading edge deposition testing. Figure 37 shows the housing that holds the faired cylinders during testing in the TuRFR, with the coolant flow noted. All of the cylinders are hollow, allowing the coolant to pass through and be discharged from the opposing cavity. Fortunately, the addition of coolant substantially reduced the thermal expansion of the cylinder wall during testing. Thus, when deposits formed at high temperature, the subsequent contraction of the metal

during shutdown was reduced and the deposits were more resilient. Figure 38 shows a post-test image of four 0.5" diameter faired cylinders with cooling applied.

Figure 39 shows a side-by-side comparison of deposits on the 0.5" cylinders and on a CFM56 vane doublet. For this test, the cylinders were canted at 50degrees to the flow direction. The operating conditions for the two tests were very similar in terms of gas temperature (2000°F), gas flow rate (0.8 lbm/sec), and particulate loading (100-125 grams). The ash types are not the same; the CFM56 vanes were tested with a sub-bituminous ash while the cylinder tests were with lignite. This explains the difference in color. Despite this, there are several similarities between the two results. (1) The deposits are thickest at the leading edge. (2) The deposit thickness rapidly tends to zero on the suction surface, with the majority of deposition occurring on the stagnation region and pressure surface. There are also significant differences. The deposits on the CFM vane are thicker and display more variability in structure (roughness).

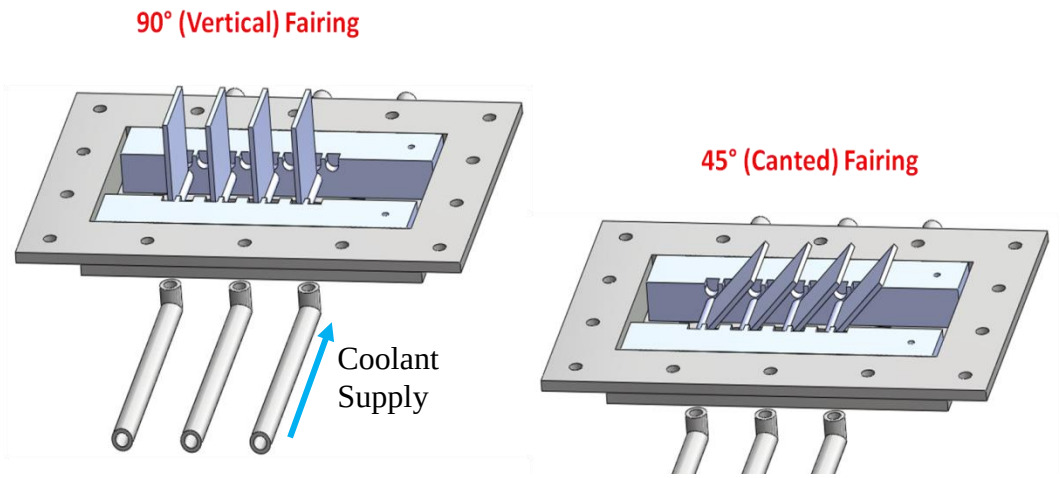

Figure 37: Installation of the faired cylinders during testing

Figure 38: Post test image of 0.5" diameter cylinders with deposition intact. Internal cooling was used to limit thermal expansion.

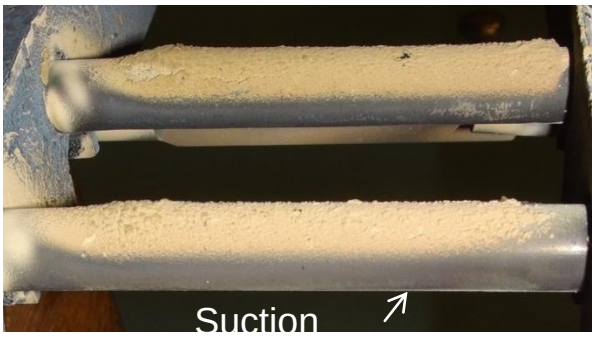

(a) 0.5" Faired Cylinders **(b) CFM56 Vane Doublet**

Figure 39: Deposition on cylinders vs. vanes.

There are several possible explanations for the differences between the vane and cylinder deposits: ash type, geometry, and/or film cooling holes. These were each evaluated as follows. A review of testing with multiple ash types on the CFM56 ruled out the ash type as a probably cause. Tests with lignite and sub-bituminous on the CFM show no significant difference in structure, though the lignite does deposit more readily at a lower temperature. The two geometries are different in two significant ways: the leading edge diameter and the flow path. The effective leading edge diameter for the CFM56 vane is approximately 0.75" vs. 0.5" for the faired cylinder. The CFM flowpath experiences more turning and does not have the abrupt weld bead which is evident at the junction between the cylinder and the fairing on the faired cylinder. While these could have a first order effect on deposition, it was suspected that the film holes are actually more responsible for the observed differences in deposition from the vane to the cylinder. Video footage of deposition in process for the vanes shows that deposits initially form at film hole sites. With time the deposits then coalesce to form the full vane coverage shown in Fig. 39b. The deposit surface structure may therefore be due to the formation process itself.

Based on this observation, it was determined that the best means to fully investigate the effect of film cooling holes is to fabricate a vane model without film holes. As such, a research vane design contributed by Rolls Royce was incorporated into a vane test section that was fabricated for testing in the TuRFR. Figure 40 shows the vane model and Figure 41 shows the final vane "quad" after a deposition test. A leading edge cooling hole was incorporated in each of the 4 vanes such that internal cooling can be applied, as with the faired cylinders. Also, the 2nd vane from the left has a film cooling slot EDMd into it for the Phase 3 study. Numerous tests with the new vanes without film cooling holes did indeed verify that the deposit structures on the vanes were similar to those on the faired cylinders for the same leading edge diameter (compare Fig. 41 and Fig. 38).

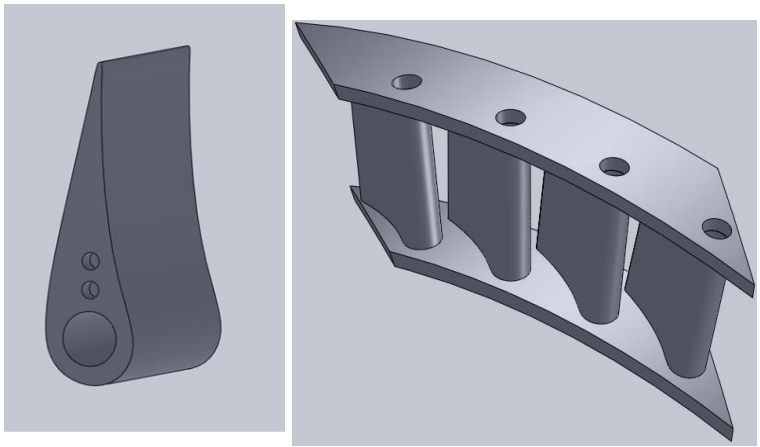

Figure 40: Rolls-Royce vane model

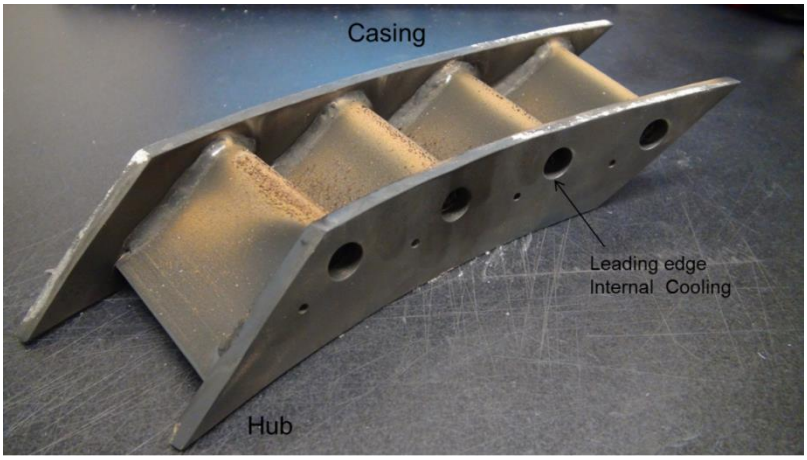

Figure 41: Rolls Royce vanes

Effect of Leading Edge Diameter

Three different tests conducted with faired cylinders finalized conclusions on the effect of leading edge diameter on deposition. Complications of deposit spallation continued to hamper this evaluation, so different techniques were used to gather information on the thickness of deposits. Initial conclusions suggested that the smaller diameter leading edge accumulates deposits at an increased rate. Using the definition of Stokes number shown in Equation 1, where the cylinder diameter is found in the denominator, one can expect that particles approaching the smaller diameter cylinder will have a larger effective Stokes number compared with the same particles approaching the larger cylinder, if all other variables are held constant.

$$St = \frac{\rho_p D_p^2 U_{in}}{18 \mu_{in} D_{LE}} \quad \textbf{(1)}$$

A larger Stokes number suggests that the trajectory of the particles is governed more by ballistics rather than fluid dynamics. In other words, the larger cylinder diameter has a greater upstream influence on the flow than the smaller counterpart. This will cause the flow streamlines to begin deviating from their straight-line trajectory further upstream, hence increasing the probability that the particles will miss the leading edge of the cylinder or avoid a direct hit with the surface. The net result is an expected reduction in the probability of sticking. Computational simulations were run to validate this theory using a particulate-laden flow approaching a cylindrical leading edge where the Stokes number was varied. The results can be found in Figure 42. As seen experimentally, increased deposition is predicted with increasing Stokes number. Previous deposition tests on CFM56 vanes demonstrated the effect of Stokes number on deposition thickness (Fig. 43). The Stokes number was varied by grinding the ash down to smaller sized particles. Size distribution for unground, 96hr, and 120hr grind are available in Figure 44. From Fig.43, it is evident that larger Stokes led to thicker deposits on the CFM vanes due to higher probability of particle impacts.

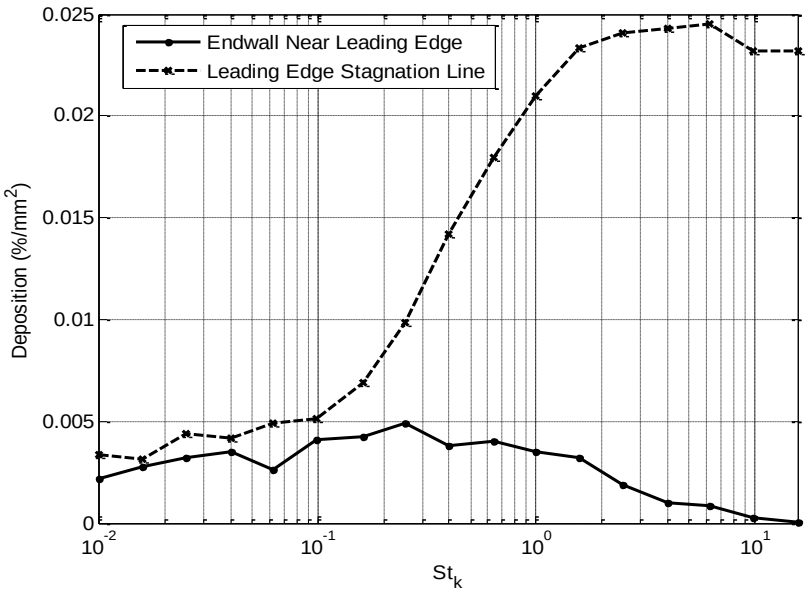

Figure 42: Computational simulation to predict deposition on a cylinder with varying Stokes number

Figure 43: Deposits on CFM56 vanes for different Stokes numbers

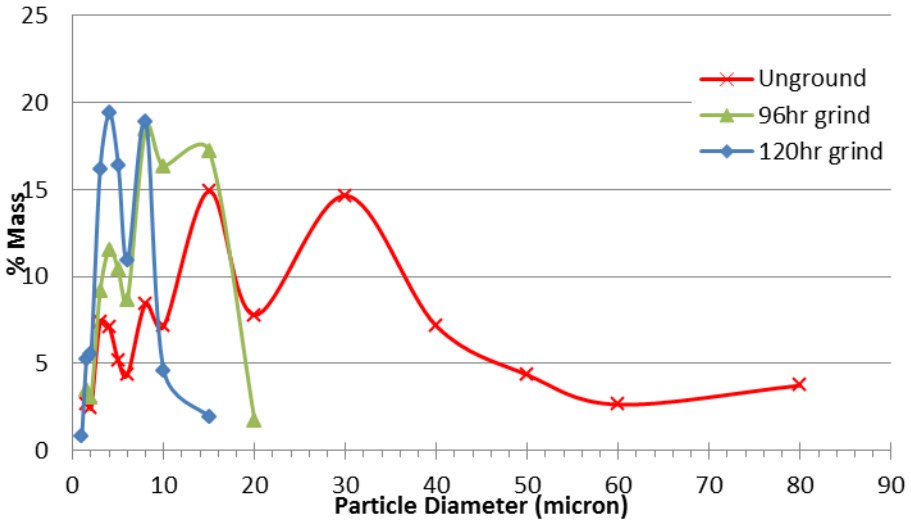

Figure 44: JBPS particle size distribution

Laser scans of the vanes before and after the test confirm that thicker deposits formed in tests with higher Stokes number. Figure 45 shows surface normal deposit thickness vs. vane wetted distance for two Stokes numbers. Notice the thickness is normalized by the amount of ash injected in order to account for any variability from test to test. Results from two independent tests at similar operating conditions for each Stokes value demonstrate good repeatability. Because the smaller Stokes particles follow the flow streamlines more closely, there are considerably fewer surface impacts and thus deposition is substantially reduced. Most of this reduction occurs at mid-chord on the pressure surface, where the flow turning has been mostly completed and passage streamlines are aligned parallel to the wall. However, even the leading edge region experiences up to a 50% reduction in deposits.

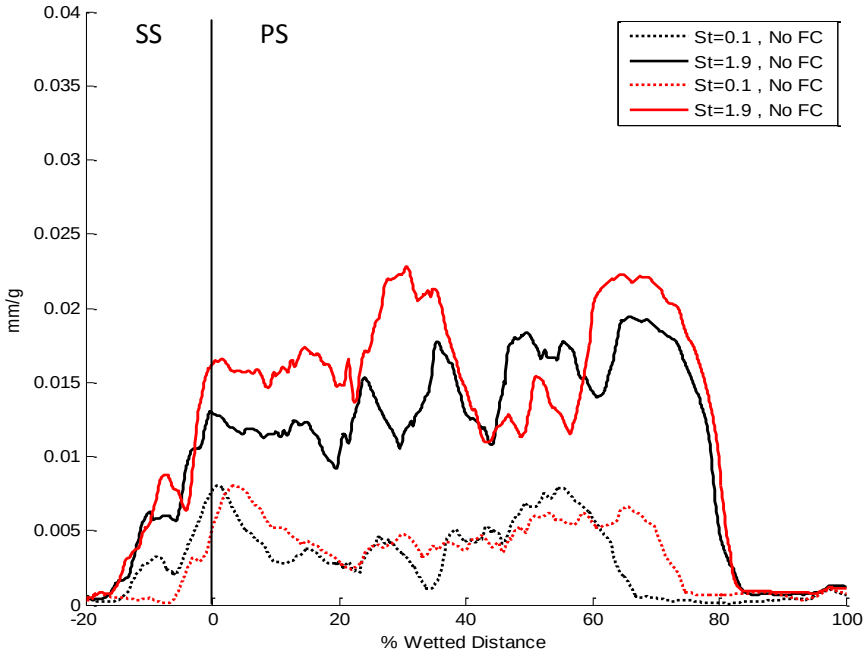

Figure 45: Surface normal deposit thickness vs. wetted distance for 2 Stokes numbers

Having established that initial deposits occur more readily on a smaller diameter leading edge, we then considered what happens as deposits begin to build on the surface. As deposits thicken on both cylinders, the larger cylinder provides a more stable platform for deposits to accumulate and thicken. Due to the increased radius of curvature, local shear forces on the newly formed deposits are not as intense and accumulation can continue to a larger absolute thickness. Figure 46 presents a schematic of large scale deposit on cylinders of different diameter, based on experimental observations and modeling. Deposit formation and structure is very similar on both cylinders. The thickest region of the deposits is found at the stagnation point. The thickness quickly drops to zero downstream of the stagnation line as the impact angle of ash particles becomes very shallow and shearing forces reduce sticking. The larger cylinder, with a larger radius of curvature, allows for a larger area where deposits can form and as a result the absolute thickness is greater than that of a smaller cylinder. This pattern can be seen in Fig. 45 for the CFM56 vanes. Deposit thickness quickly drops from the stagnation line towards the suction surface.

Three tests were conducted to study deposition during the initial growth of deposits before equilibrium between shearing and deposition is reached. All tests used JBPS ash and no cooling. It was decided to exclude cooling from the test to ensure all cylinders had the same surface temperature and prevent any bias in the deposition. Figure 47 shows a photograph of the post test results of the three tests. In Test 1, shown in Fig 47a, unground JBPS ash with a median diameter of 12 microns was used. For Test 2 and 3 a ground version of the same ash was used which dropped the median diameter to 4 microns. These two tests experienced significant deposit spallation which made it difficult to obtain accurate thickness measurements, especially from Test 2. Ground ash was used to drop the Stokes number below one where Figure 7 predicts greater differences in deposition rates exist.

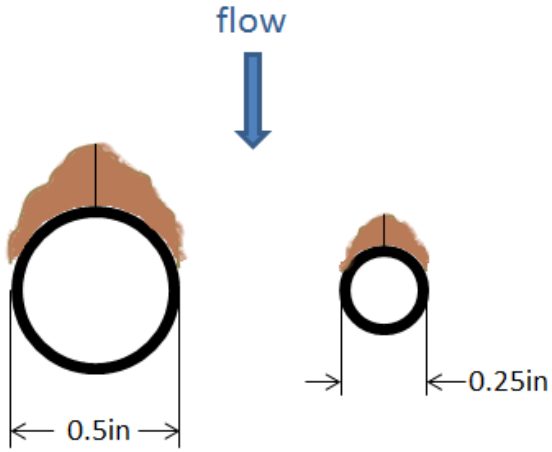

Figure 46: Schematic of large scale deposition on cylinder

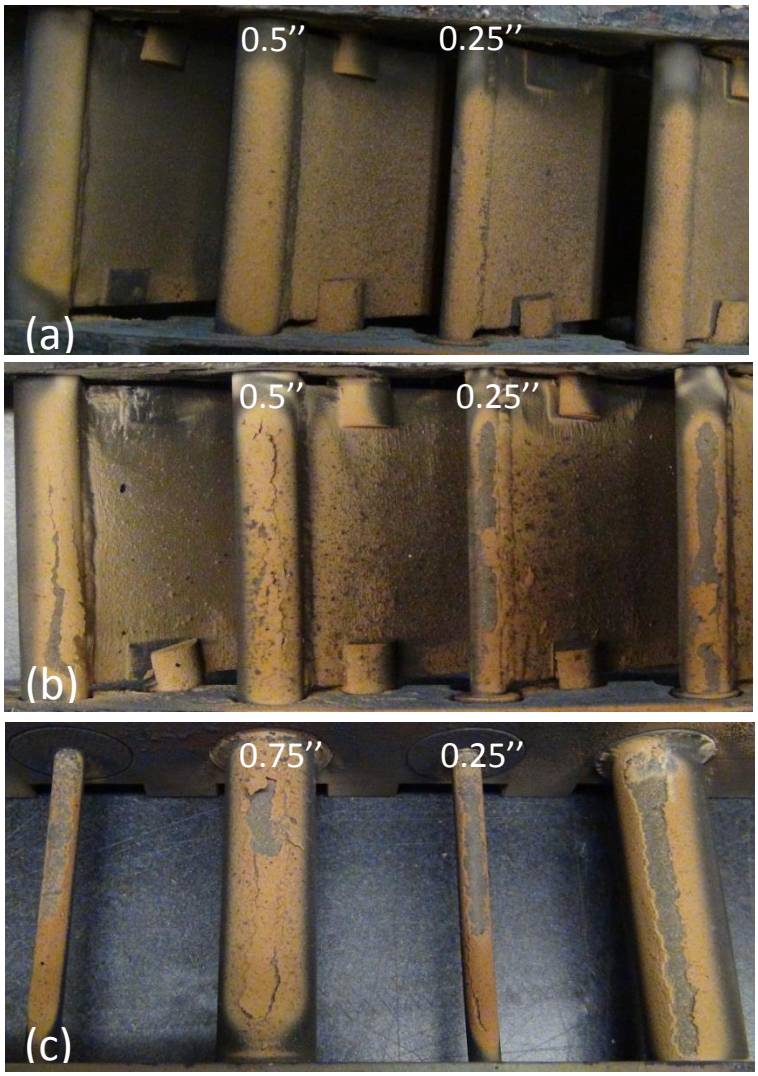

Figure 47: TuRFR deposition tests with various cylinder diameters. Post test images
(a) Test 1 (b) Test 2 (c) Test 3

Table 2 shows the test condition for each test and Table 3 lists the Stokes number for each cylinder in each test. For Test 3 it was decided to use a larger cylinder with a diameter of 0.75 inches in order to provide a greater difference in Stokes number. This cylinder is not available with a fairing, so all of the cylinders used in this test were without fairings.

Table 2: Test Conditions

	Test 1	Test 2	Test 3
Mass Flow (lbm/s)	≈ 0.4		
Inlet Vel. (m/s)	≈ 65		
Flow Temp. (oF)	≈ 2000		
Ash Loading (g)	12.9	32.4	46.6
Ash Type (JBPS)	Unground	120hr grind	
MMD (micron)	12	4	4

Table 3. Stokes number for all tests

	Stokes Number		
Test	0.25" LE Dia.	0.5" LE Dia.	0.75" LE Dia.
1	5.4	2.7	--
2	0.38	0.19	--
3	0.38	--	0.13

Deposit thickness was measured at the stagnation region for Test 1 and 3. No results were obtained from Test 2 due to the large amount of deposit loss. Figure 48 shows an image taken of the 0.5in cylinder in Test 1 which was used to measure the thickness of deposits at the stagnation region.

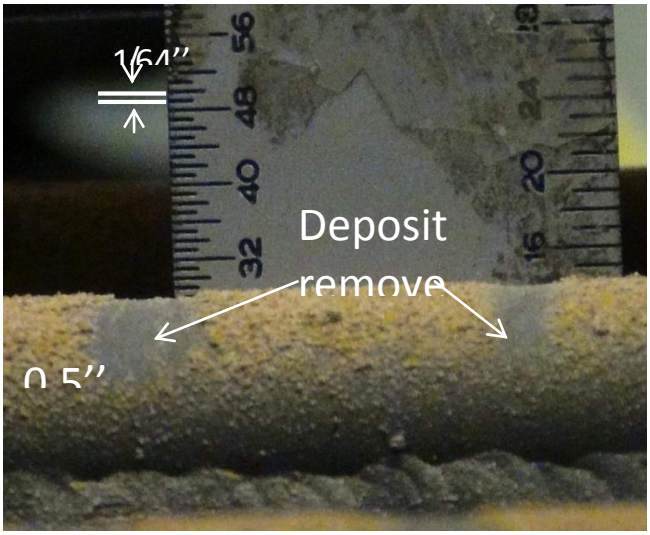

Figure 48: Deposit thickness on 0.5in diameter cylinder (Test 1)

The technique shown in Figure 48 was used to measure the thickness of the deposit and acquire a difference between the 0.25'' and 0.50'' cylinder. For Test 3, the deposit thickness was physically measured since it had lifted off the surface during the cooling down phase of the test. Results are listed in Table 4.

Table 4: Deposit thickness in stagnation region

	Deposit Thickness (inches)			
Test	**0.25**	**0.5**	**0.75**	**Diff**
1	0.012	0.01	--	0.002
3	0.016	--	0.012	0.004

From the measurements in Table 4, it is observed that thicker deposits are consistently found on the smaller cylinder, where the Stokes number is larger and more particle impacts are expected to occur. Test 3, which had a Stokes number below one for both cylinders, shows greater deposit thickness difference between the smaller and larger cylinder. This trend is expected to be true only during initial build up. After this period the larger diameter, with a larger radius of curvature, provides a more stable platform for continuing deposit build up.

The deposits on these cylinders were laser scanned for transmission to University of North Dakota. Figure 49 shows the raw data from the scan for the 0.5 inch cylinder with and without deposits.

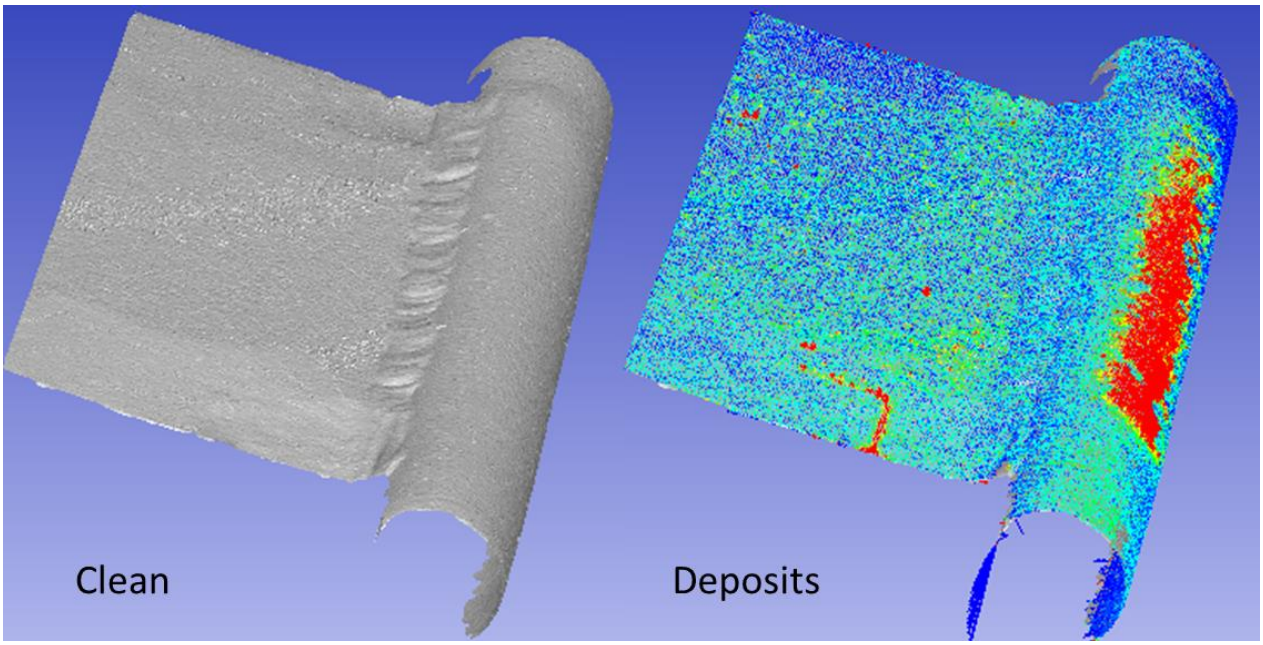

Figure 49: UDRI 0.5 inch cylinder scans: clean vs. deposits

PHASE 2

This section of the report summarizes results from the study of the effects of turbulence on deposition rates. A detailed account of this study was presented in a conference paper at the 2014 IGTI Conference in Dusseldorf, Germany (Whitaker, S.M., Prenter, R., and Bons, J.P., 2014, "The Effect of Freestream Turbulence on Deposition for Nozzle Guide Vanes", presented at the ASME Turbo Expo 2014 in Dusseldorf, Germany, June 16-20, 2014. Paper #GT2014-27168.)

In order to modify the flow turbulence, a stainless steel grid (shown in Figure 50) was designed that could be inserted into the TuRFR upstream of the vanes, as seen in Figure 51. The grid is comprised of several welded circular cylinders with diameters of 6.35 mm, with 19 mm spacing between the cylinder centerlines. The area blockage was designed to be approximately 50 percent. When installed, the grid sits

approximately 24 cylinder diameters upstream of the vane inlet plane. The grid's design was guided by previous work from Roach [1].

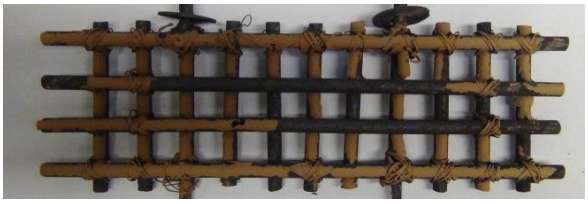

Figure 50: Turbulence Grid

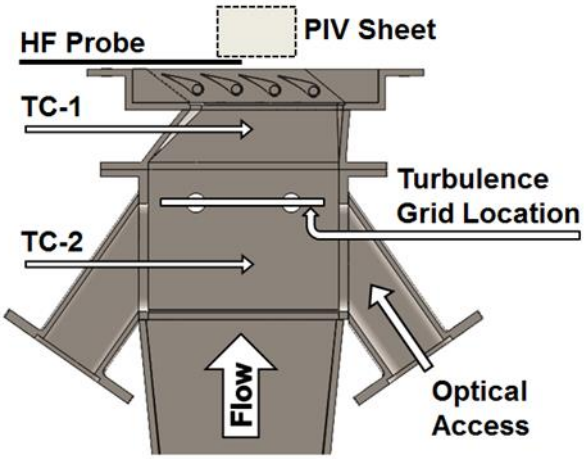

Figure 51: Diagram of TuRFR Top Section with Instrumentation and Grid Location

Turbulence measurements for non-reacting flow in the TuRFR using hot film anemometry show that the flow turbulence actually decreases with the grid installed from a background turbulence level of approximately 6 percent to 4% (at nominal massflow rates). PIV measurements of the flow turbulence were also taken for both reacting and non-reacting flow. For the non-reacting flow, PIV appeared to underestimate the background turbulence (relative to hotwire) and overestimate the grid turbulence. With the combustor operating (reacting flow), PIV registered a background turbulence level approaching 9-10% (up from 6% for non-reacting). The grid turbulence measured by PIV was 6%. Comparable measurements have been reported elsewhere [2-5].

All the above measurements were taken without the vanes installed. An upgraded TuRFR top section installed in early 2014 allowed the measurement of inlet turbulence levels using a hot wire anemometer (again for non-reacting flow). The presence of the vanes resulted in a slight increase in the measured turbulence intensity.

A series of tests were performed to characterize the effect of turbulence on deposition. Two ash size distributions (mass median diameter of 4.6 and 6.5μm) were used. After each test was completed, the ash was removed and measured in order to assess the relative rates of deposition between the tests at different turbulence levels. The capture efficiency (a ratio of deposited ash to injected ash) was measured and is plotted in Fig. 52 vs. turbulence intensity for the two ash sizes (MMD).

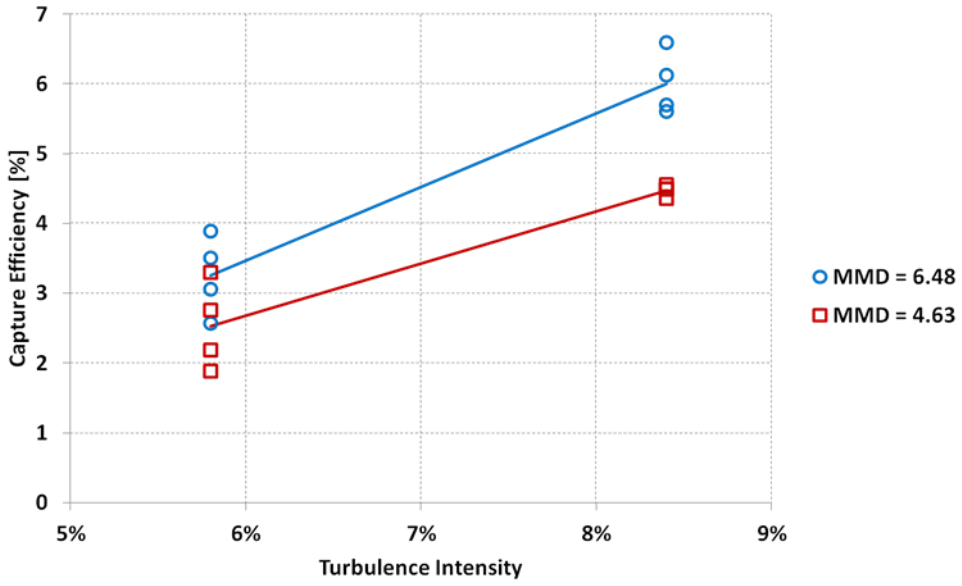

Figure 52: Capture Efficiency Versus Turbulence Intensity for Different Ash Sizes. Solid Lines Connect Mean Values of each Cluster.

It is observed that a 50 percent increase in the free-stream turbulence (from 5.8 percent to 8.4 percent for grid in to grid out operation) results in a 77 percent increase in capture efficiency for the 4.63 µm ash, and a 84 percent increase for the 6.48 µm ash. Based on a Stokes number analysis of how the particulate should react to flow turbulence, we would expect the ash with an increased number of smaller particles (those with lower Stokes numbers) to be more affected by the flow turbulence than the ash with larger particles. The experimental results do not support this analysis. It is possible that the turbulent diffusion mechanism, which acts to deliver particles to the surface, is negated by the damping of turbulent fluctuations near the wall. Particles with large Stokes numbers may be perturbed by the flow turbulence and have enough inertia to maintain a ballistic trajectory through the boundary layer, where the turbulent fluctuations are damped. Particles with small Stokes numbers that are perturbed toward the vane surface may lack the inertia required to overcome the damping within the boundary layer. Consequently, the capture efficiency for small particles would be less affected by turbulent fluctuations in the free-stream. This implies that a non-monotonic variation in capture efficiency with particle size might be expected.

Modeling of Deposition and Turbulence

This CFD simulation (using Fluent) was performed using the TuRFR vane geometry incorporated as a single passage, as well as the flow conditions observed during experiments (including temperature, Mach number, turbulence intensities, and particle size distributions). The mesh geometry is shown in Fig. 53. Deposition was simulated using a sticking model implemented as a user-defined function. Turbulence was modeled using the k-ω SST model using the turbulence values obtained from experiments. The trajectory of particles was predicted using the Discrete Phase Model in Fluent and turbulent diffusion was modeled using the stochastic discrete random walk model.

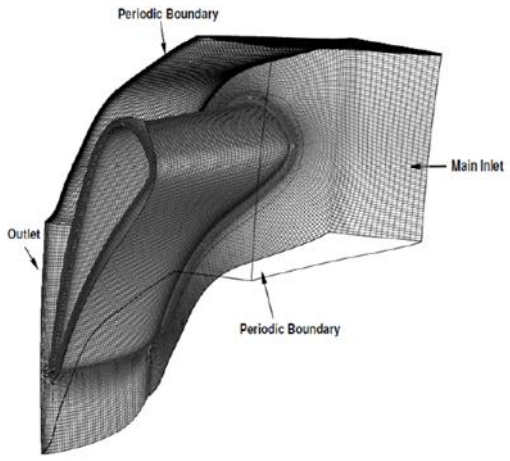

Figure 53: Mesh Geometry for CFM56 Vanes. Note that the mesh aspect ratio has been skewed to protect the proprietary nature of the geometry.

To assess how well the computation models the turbulent dispersion of particulate, the mass-based impact efficiency was examined. This parameter provides the mass of particles that impact the vane relative to the total mass injected for a given particle size. Assuming the only variation in the experiments is the turbulence level, this parameter should vary in the same manner as the capture efficiencies obtained from the experiment. Indeed, the model did predict an increase in impact efficiency with increased turbulence, similar to the experiment. Fig. 54 shows the capture efficiency ratio (high to low turbulence) from the experiment alongside the impact efficiency ratio data from the Fluent simulation.

It is noted that the computational results indicate that smaller particles should be more affected by a change in the free-stream turbulence level. This follows the Stokes number analysis discussed previously, but runs contrary to the experimental observations. In addition, the predicted increase in mass-based impact efficiency for the 6.48 micron ash is much lower than that observed in the experiments. These results indicate that the Discrete Phase Model may not capture all of the relevant physics associated with particle transport in turbulent flows.

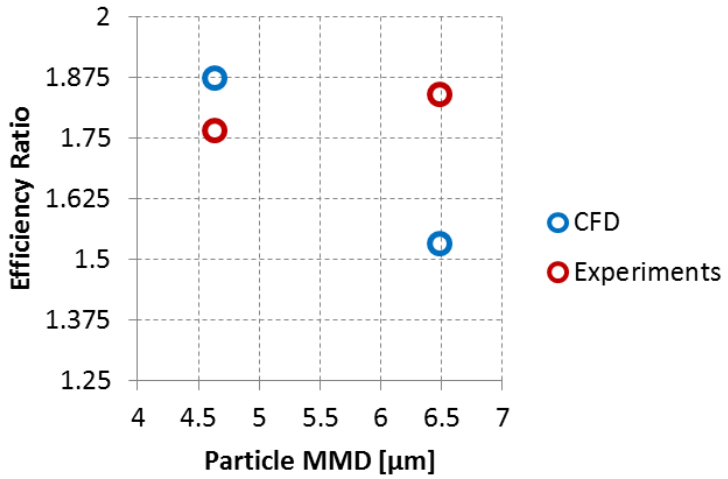

Figure 54: Ratio of capture (or impact) efficiency plotted vs. particle size (MMD) for experiments and CFD.

PHASE 3

To meet the research objectives of Phase 3, testing and analysis were conducted to understand the role of film cooling on deposition. This effort is described in detail in a conference paper presented at the 2014 IGTI Conference in Dusseldorf, Germany (Prenter, R., Whitaker, S.M., and Bons, J.P., 2014, "The Effects of Slot Film Cooling on Deposition on a Nozzle Guide Vane", accepted for presentation at the ASME Turbo Expo 2014 in Dusseldorf, Germany, June 16-20, 2014. Paper #GT2014-27171.). Tests were strategically conducted to help shed light on some major questions; namely, the role of surface temperature and the role of injecting particle-free coolant.

Slot Cooling with Deposition

The design and manufacturing of the annular test piece was described previously, a schematic of the piece is provided in Fig. 55 for convenience. The diagram indicates which side coolant enters, as well as the vane numbering convention used in this report. To investigate the effect of slot film cooling on deposition, several tests were run at varying coolant flow rates. The vane inlet conditions, 0.363 kg/s and 1339 K, were kept constant during and between tests. Table 5 summarizes the nominal test conditions.

Coolant mass flow rate was held constant during each test, with several flow rates tested. The coolant is not actively heated, but is rather passively heated by the facility to reach a cooling cavity inlet temperature that depends on coolant flow rate. This temperature was measured for each coolant mass flow rate, and is accounted for in the results.

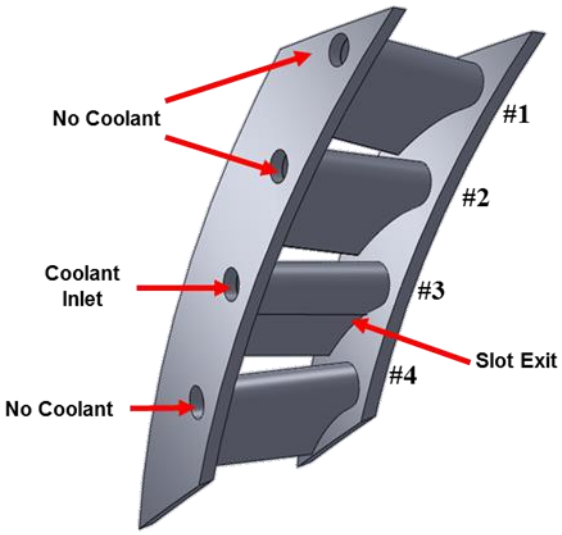

Figure 55: Schematic of the annular test section

Table 5: Test conditions

Inlet Mass Flow Rate	0.363 kg/s
Nominal Inlet Flow Temp.	1339 K
Inlet Mach Number	0.1
Exit Re based on chord	152,000
Inlet Re based on LE diameter	8,509

There are several important parameters useful in characterizing the coolant flow. The first of these are density ratio and blowing ratio,

$$DR = \frac{\rho_c}{\rho_\infty} \qquad M = \frac{\rho_c u_c}{\rho_\infty u_\infty}$$

Note that because the slot has a large L/h ratio, there is a substantial amount of heat pick up in the slot passage, and the parameters above will have significantly different values when referencing the cooling cavity inlet conditions and the slot exit conditions (for the numerator). Both values are thus reported. The exit values were estimated from the computational solution at midspan as local exit conditions could not be measured. These values, as well as the coolant-passage mass flow rate ratio $\dot{m}_c/\dot{m}_p$, Reynolds number based on slot height h, Re_h, and cooling cavity inlet temperature, are listed in Table 5 for each cooling level.

As coolant mass flow rate and temperature were varied between tests, a new variable is introduced to better capture the differences between tests and allow for comparison to other studies that have different facilities and test articles. The non-dimensional thermal capacity ratio is defined as,

$$\Phi = \frac{\rho_c u_c A_c (T_\infty - T_{c,i})}{\rho_\infty u_\infty A_s T_\infty}$$

where ρ_c, u_c, A_c are the density, velocity and area at the slot exit. The temperature $T_{c,i}$ is the coolant temperature at the inlet to the cooling cavity. The variables with the '∞' subscript are all evaluated in the free stream, and A_s is the area of the surface being cooled. This parameter allows comparison of experiments with different free stream and coolant conditions, as well as different cooled-surface sizes (through A_s). The product $\rho_\infty u_\infty A_s$ scales with passage mass flow rate (or equivalent depending on the respective facility), thus Φ gives a measure of the thermal capacity ratio between the coolant and free stream. The thermal capacity ratio corresponding to each coolant mass flow rate is also listed in Table 5.

Table 5: Cooling parameters

$\frac{\dot{m}_c}{\dot{m}_p}$ %	$T_{c,i}$ [K]	Re_h	$DR(DR_{in})$	$M(M_{in})$	Φ
0.62	926	172	1.13(1.54)	1.16(1.58)	0.00139
0.88	834	274	1.21(1.74)	1.74(2.50)	0.00245
1.27	705	434	1.30(2.31)	2.67(4.37)	0.00443

Coolant Characterization Revisited

The characterization of the coolant flow using infra-red imaging is shown in Fig. 56 for each flow rate, with chordwise linear traces of surface temperature at mid-span presented in Fig. 57.

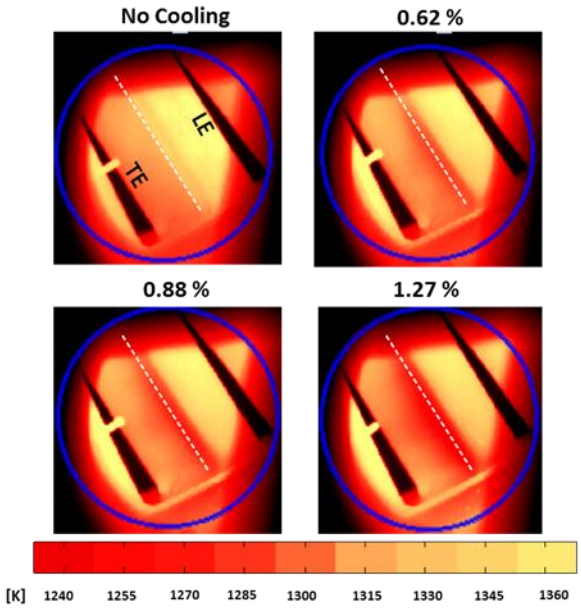

Figure 56: IR images of the pressure surface at different mass flow ratios. Coolant enters from the lower right hand side of the vane.

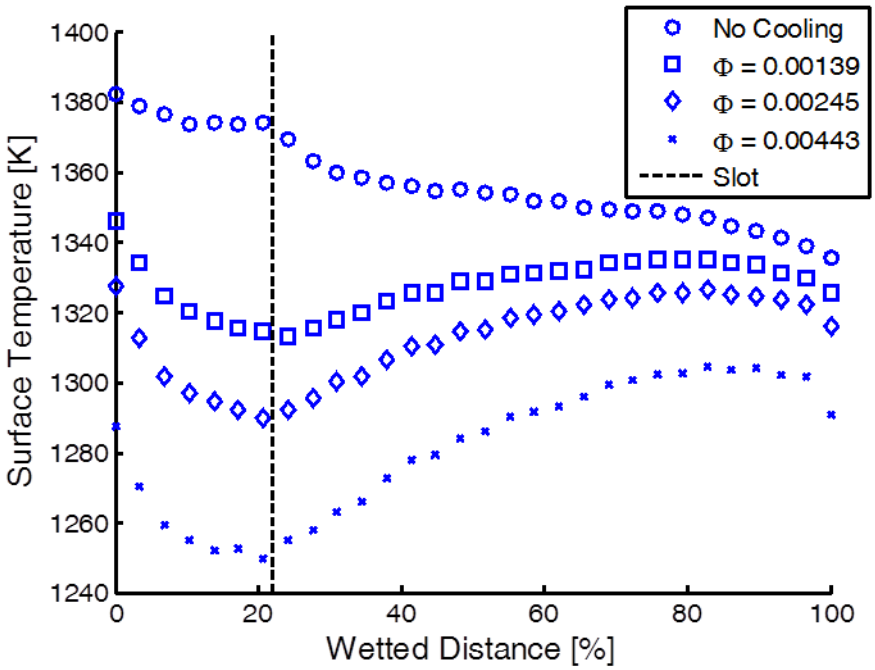

Figure 57: Chordwise linear traces of surface temperature at mid-span.

As the coolant temperature at the inlet to the cooling cavity varies with coolant flow rate (the coolant is passively heated by the facility), the traces presented in Fig. 57 do not provide a correct indication of the effect of increasing coolant mass flow rate. A non-dimensional parameter was defined to account for both the coolant inlet temperature and local variations already present in the baseline,

$$\theta = \frac{T_{St} - T_{s,c}}{T_{s,b} - T_{c,i}} - \frac{T_{St} - T_{s,b}}{T_{s,b} - T_{c,i}} = \frac{T_{s,b} - T_{s,c}}{T_{s,b} - T_{c,i}}$$

where T_{St} is the stagnation temperature, $T_{s,b}$ is the surface temperature for the baseline non-cooled test, $T_{s,c}$ is the surface temperature for the cooled test investigated, and $T_{c,i}$ is the respective coolant inlet temperature. By normalizing the temperature difference by the relevant coolant inlet temperature and subtracting the baseline term, this parameter provides the cooling effectiveness relative to the local baseline temperature and respective coolant inlet temperature. The new parameter is plotted in Fig. 58 in chordwise traces for each coolant mass flow ratio. The trends are similar to those discussed for surface temperature, though it is interesting to note that the highest effectiveness is achieved upstream of the slot. This characteristic is also observed in the experimental deposition results and conjugate heat transfer calculations.

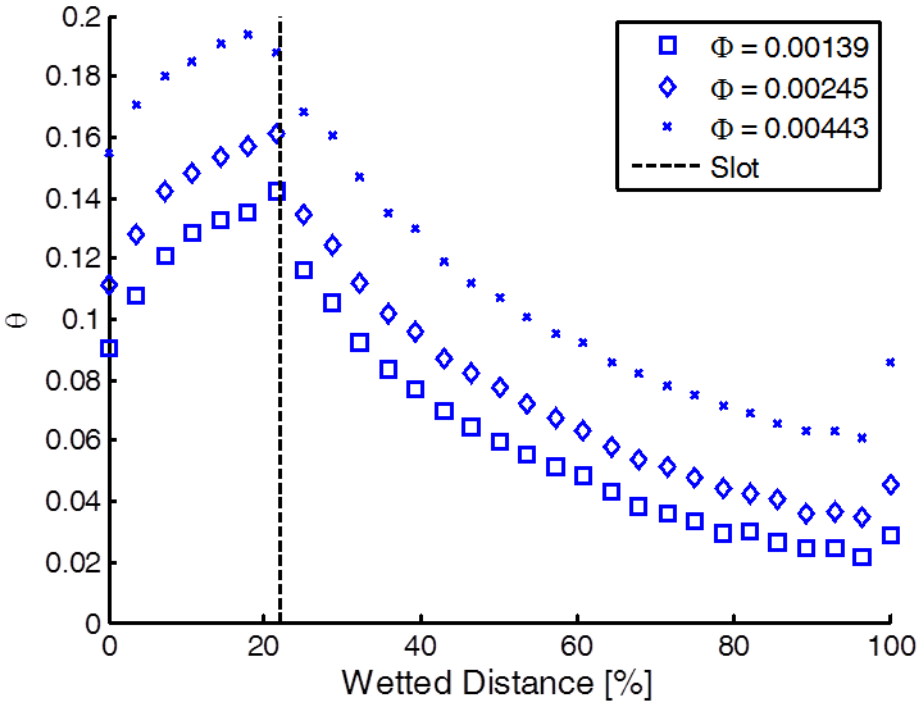

Figure 58: Chordwise linear traces of surface temperature at mid-span

Experimental Deposition Tests

Experimental external deposition tests were conducted at the three coolant mass flow rates, as well as a non-cooled baseline case. All other test conditions were held constant between each test. Photographs shown in Fig. 59 compare a no-cooling baseline test to the highest cooling level test. Surface scans of both vanes for each cooling level are presented in Fig. 60 with representative linear chordwise traces shown in Fig. 61.

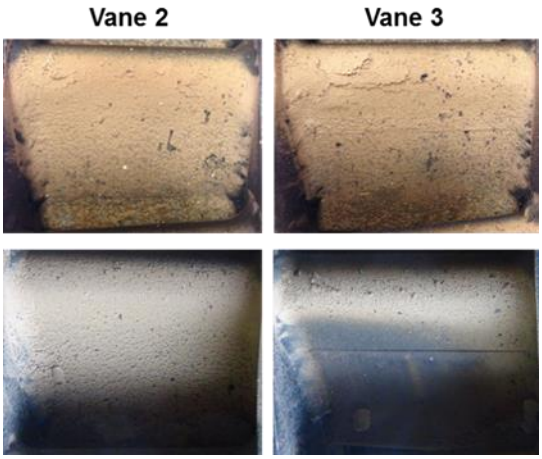

Figure 59: Photographs comparing non-cooled case (top) to $\Phi = 0.00443$ case (bottom). Coolant enters on the left hand side of Vane 3

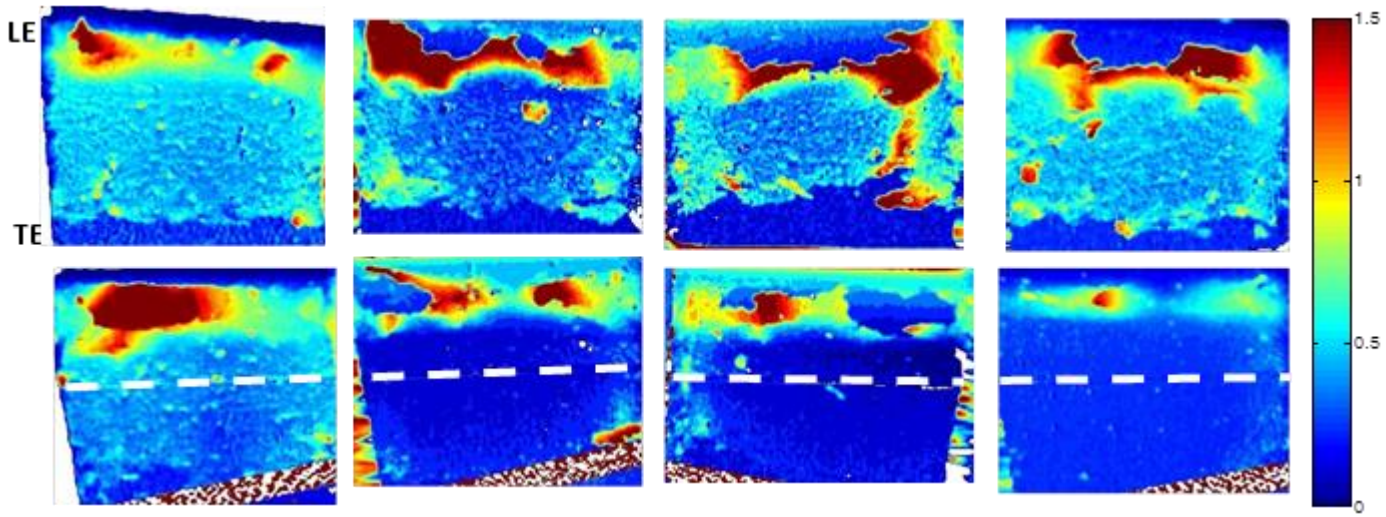

Figure 60: Scans of uncooled Vane 2 (top) and cooled Vane 3 (bottom) from deposition tests, left to right: Baseline, $\Phi = 0.00139$, $\Phi = 0.00245$, $\Phi = 0.00443$

Bonilla et al. [7] conducted external deposition experiments with CFM56-5B nozzle guide vanes to examine the effect of discrete film cooling holes on external deposition. The authors compared capture efficiency data to results from Crosby et al. [6], where circular coupons were cooled only by backside impingement. In this comparison, the coolant mass flow rates reported in each study were normalized by the respective deposition-prone area of the surface being cooled to account for the differences between the two facilities. The data from each study, as well as capture efficiencies reported in this work, are plotted in Fig. 62 against Φ, which includes the cooled-surface area normalization but better accounts for the differences in free stream and coolant properties. It should be noted that since the test piece in [8] did not include film cooling, A_c was set as the cross sectional area of the duct where the backside of the coupon was cooled. It is clear that the slot film cooling scheme achieves similar reductions in capture efficiency with much lower coolant flow rates. Ai et al. [8] furthered Crosby's work by conducting deposition experiments on film-cooled coupons in the same facility. Their data is also shown in the comparison in Fig. 62.

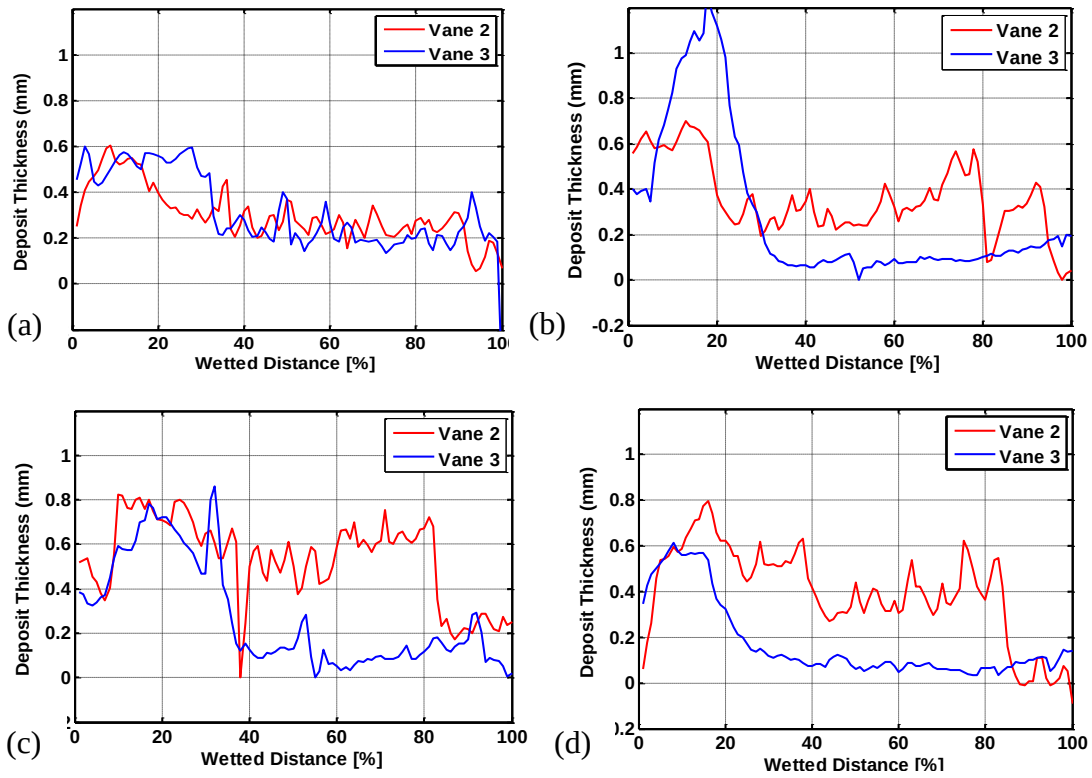

Figure 61: Linear traces of deposit thickness: (a) Baseline, (b) Φ = 0.00139, (c) Φ = 0.00245, (d) Φ = 0.00443

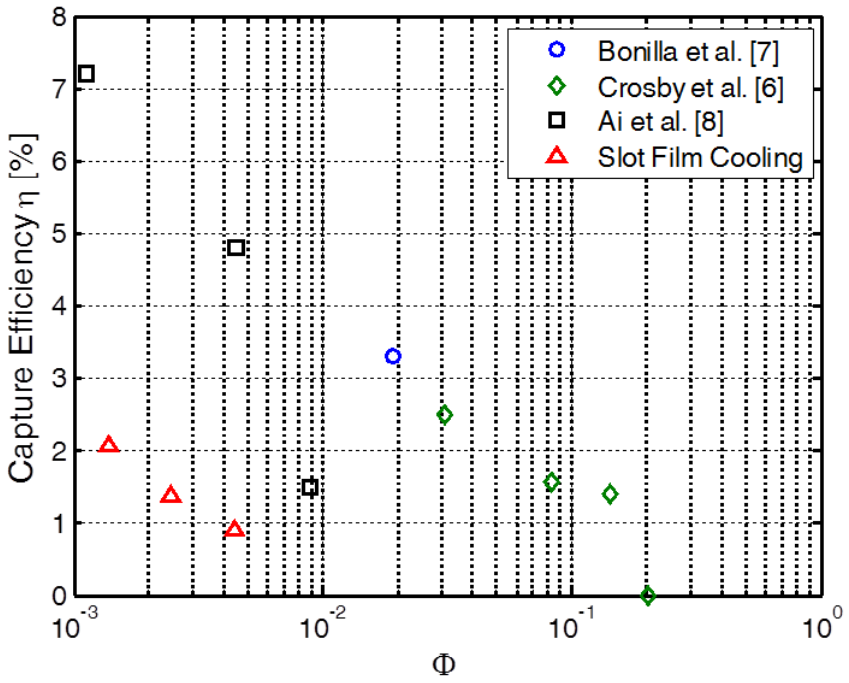

Figure 62: Comparison of capture efficiency to Crosby et al. [6], Ai et al. [8], and Bonilla et al. [7]

The inclusion of film cooling significantly reduced deposition on the coupon, with capture efficiencies closer to those found in this study. There are some other differences between the four studies that should be mentioned before making further comparisons; the ash used in [7] was lignite, which has a higher propensity to stick than JBPS ash (the ash used in this study). While [6] also used JBPS ash, the particle size distribution after grinding would most likely be different from that of the ash used in this study. The main flow and coolant temperatures were different between the four studies, though this is captured by Φ. To account for these additional differences, the capture efficiency is normalized by the capture efficiency measured for the respective baseline non-cooled case in each study, to arrive at a capture efficiency reduction factor. This is plotted in Fig. 63 for each study against area-normalized coolant mass flow rate (log scale). With differences accounted for, the slot film cooling scheme still achieves similar reduction factors using less coolant. Clearly, the slot cooling design on the vane is a significant improvement over the discrete film cooled coupons when it comes to deposition.

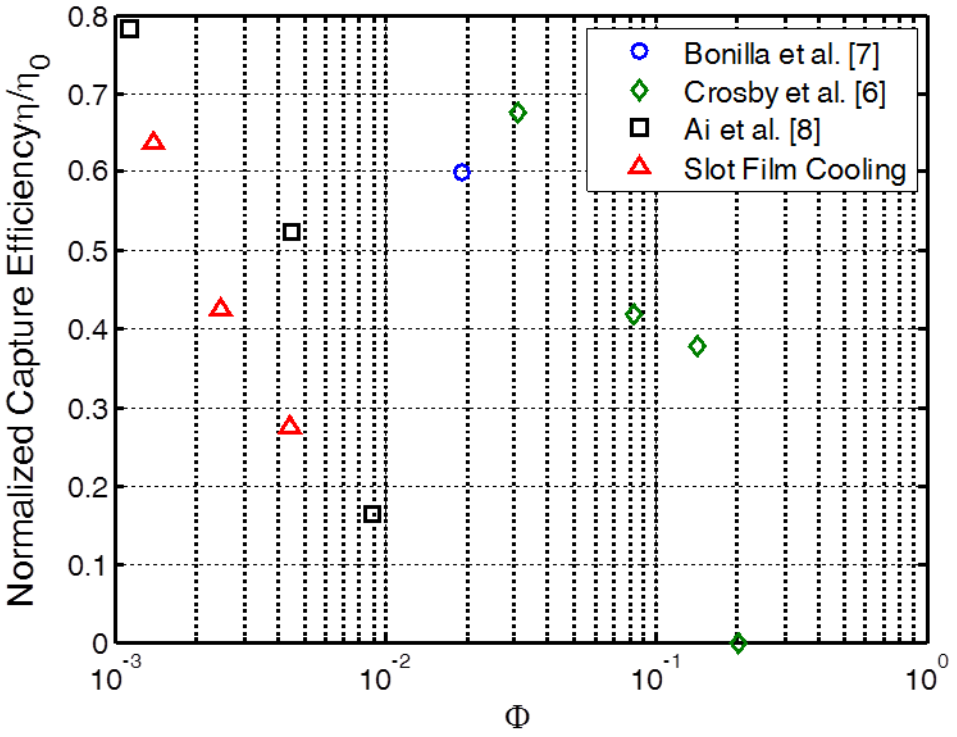

Figure 63: Comparison of normalized capture efficiency to Crosby et al. [6], Ai et al. [8], and Bonilla et al. [7]

References

[1] Roach, P. E., "The generation of nearly isotropic turbulence by means of grids" Rolls Royce Ltd 1986

[2] Lavoie, P., Avallone, G., DeGeorgio, F., Romano, G., and Antonia, R., "Spatial Resolution of PIV for the Measurement of Turbulence," *Experiments in Fluids*, Vol. 43, pp. 39-51, 2007.

[3] Saarenrinne, P., Piirto, M., and Eloranta, H., "Experiences of Turbulence Measurement with PIV," *Measurement Science and Technology*, Vol. 12, pp. 1904-1910, 2001.

[4] Goldstein, R., Lau, K. and Leung, C., "Velocity and Turbulence Measurements in Combustion Systems," *Experiments in Fluids*, Vol. 1, No. 2, pp. 93-99, 1983.

[5] Barringer, M., Thole, K., and Polanka, M., "Experimental Evaluation of an Inlet Profile Generator for High-Pressure Turbine Tests," *ASME Journal of Turbomachinery*, Vol. 129, pp. 382-393, 2007.
[6] Crosby, J.M., Lewis, S., Bons, J.P, Ai, W., Fletcher, T.H., "Effects of Particle Size, Gas Temperature, and Metal Temperature on high Pressure Turbine Deposition in Land Based Gas Turbines from Various Synfuels," ASME No. GT2007-25731.
[7] Bonilla, C., Webb, J., Clum, C., Casaday, B., Brewer, E., and Bons, J., "The Effect of Particle Size and Film Cooling on Nozzle Guide Vane Deposition" *ASME Turbo Expo 2012: Power for Land, Sea, and Air*. 2012.
[8] Ai, W., Murray, N., Fletcher, T., Harding, S., Lewis, S., and Bons, J., 2012. "Deposition Near Film Cooling Holes on a High Pressure Turbine Vane" *ASME Journal of Turbomachinery*, Vol. 134, 2012.

Additional Conclusions: The present project provided an improved understanding of the deposition process in the leading edge region. Further the present project documented the ability ot full coverage slot film cooling to help protect a surface from particle deposition. This project also documented the influence of high turbulence level, scale to diameter ratio and Reynolds number on its influence on stagnation region heat transfer augmentation. This investigation was extended to look at the response of turbulence in the presense of a very large stagnation region. Additionally, a highly versatile and effective internal cooling technology called "incremental impingement" was developed for application in the vicinity of a vane leading edge. Since "incremental impingement" is designed to terminate with a film cooling discharge, both slot and full coverage shaped hole film cooling arrangements were tested in an accelerating flow subjected to a wide range of relevant turbulence levels. Taken as a whole, the present project provides a better understanding of the leading edge deposition process as well as tools such as incremental impingement and slot film cooling to effectively ameliorate the effects of deposition in gas turbines.

7. PUBLICATIONS:

1. Gandaparavu, P., and Ames, F.E., 2012 "The Influence of Leading Edge Diameter on Stagnation Region Heat Transfer Augmentation Including Effects of Turbulence Level, Scale, and Reynolds Number," ***ASME J. Turbomachinery***, v. **135**, pp. 011008-1-8.
2. Busche, M.L., Moualeu, L.P., Tang, C., and Ames, F.E., 2013, "Heat Transfer and Pressure Drop Measurements in High Solidity Pin Fin Cooling Arrays with Incremental Replenishment," ***ASME J. Turbomachinery,* 135**, pp. 041011-1-9.
3. Chowdhury, N.H.K. and Ames, F.E., 2013, "The response of high intensity turbulence in the presence of large stagnation regions," ASME Paper No. GT2013-95055.
4. Busche, M.L., Kingery, J.E., and Ames, F.E., 2014, "Slot film cooling in an accelerating boundary layer with high free-stream turbulence," ASME Paper No. GT2014-25360.
5. Prenter, R., Whitaker, S.M., Ameri, A., and Bons, J.P., 2014, "The Effects Of Slot Film Cooling On Deposition On A Nozzle Guide Vane," ASME Paper No. GT2014-27171.
6. Whitaker, S.M., Prenter, R., and Bons, J. "The Effect of Free-Stream Turbulence on Deposition for Nozzle Guide Vanes," ASME Paper No. GT-2014-27168.
7. Kingery, J.A., Ames, F.E., 2015, "Full Coverage Shaped Hole Film Cooling in an Accelerating Boundary Layer with High Free-Stream Turbulence," ASME Paper No. GT2015-42233 (Accepted for presentation and publication recommended for journal publication).
8. Kingery, J.A., Ames, F.E., 2015, "Stagnation Region Heat Transfer Augmentation At Very High Turbulence Levels," ASME Paper Number: GT2015-42420 (Accepted for presentation and publication recommended for journal publication).